Report No. CG-D-22-96

# Potential of Advanced Very High Resolution Radiometer (AVHRR) Derived Sea Surface Currents for U.S. Coast Guard Search and Rescue Application

J. E. Dick O'Donnell
and
R.Q. Robe

U.S. Coast Guard
Research and Development Center
1082 Shennecossett Road
Groton, CT 06340-6096

DISTRIBUTION STATEMENT A
Approved for public release;
Distribution Unlimited

DTIC QUALITY INSPECTED 4

FINAL REPORT
April 1996

This document is available to the U.S. public through the
National Technical Information Service, Springfield, Virginia 22161

Prepared for:

19961226 097

U.S. Department of Transportation
United States Coast Guard
Office of Research and Development
Washington, DC 20593-0001

# NOTICE

This document is disseminated under the sponsorship of the Department of Transportation in the interest of information exchange. The United States Government assumes no liability for its contents or use thereof.

The United States Government does not endorse products or manufacturers. Trade or manufacturers' names appear herein solely because they are considered essential to the object of this report.

The contents of this report reflect the views of the Coast Guard Research & Development Center. This report does not constitute a standard, specification, or regulation.


G.T. Gunther
Commanding Officer
United States Coast Guard
Research & Development Center
1082 Shennecossett Road
Groton, CT 06340-6096

Technical Report Documentation Page

| 1. Report No. | 2. Government Accession No. | 3. Recipient's Catalog No. |
|---|---|---|
| CG-D-22-96 | | |

| 4. Title and Subtitle | 5. Report Date |
|---|---|
| Potential of Advanced Very High Resolution Radiometer (AVHRR) Derived Sea Surface Currents for U.S. Coast Guard Search and Rescue Application | April 1996 |
| | 6. Performing Organization Code |
| 7. Author(s) J.E. Dick O'Donnell and R.Q. Robe | 8. Performing Organization Report No. R&DC 09/96 |
| 9. Performing Organization Name and Address<br>U.S. Coast Guard<br>Research and Development Center<br>1082 Shennecossett Road<br>Groton, Connecticut 06340-6096 | 10. Work Unit No. (TRAIS) |
| | 11. Contract or Grant No. |
| | 13. Type of Report and Period Covered<br>Final Report |
| 12. Sponsoring Agency Name and Address<br>Department of Transportation<br>U.S. Coast Guard<br>Office of Research and Development<br>Washington, D.C. 20593-0001 | 14. Sponsoring Agency Code<br>Commandant (G-NRS)<br>USCG Headquarters<br>Washington, D.C. 20593-0001 |

15. Supplementary Notes

This report is the seventeenth in a series that documents the Improvement of Search and Rescue Capabilities (ISARC) Project at the USCG R & D Center. The R&DC technical point of contact is Dr. J.E. Dick O'Donnell, 860-441-2741.

16. Abstract

The U.S. Coast Guard evaluated the potential of AVHRR for estimating the near real-time surface velocity field for oceanic searches. By comparing sequential AVHRR images, the movement of sea surface temperature features can be detected from which the surface currents are inferred. Two methods are available for estimating surface currents from satellite imagery: feature tracking and inversion of the heat equation. The two techniques were evaluated to determine which method was best suited to fulfill the unique operational requirements of the U.S. Coast Guard Search and Rescue program. Implementation of these methods for operational search planning involves different requirements than for pure research. To address these issues, AVHRR derived surface currents were compared with drifting buoy measurements. It is anticipated that AVHRR imagery will be used in conjunction with imagery from other satellite sensors as the technology and data become available. In addition to providing near real-time velocity fields, the data contined in AVHRR images are useful to search and rescue operations by providing positions of thermal fronts and ocean eddies.

| 17. Key Words | 18. Distribution Statement |
|---|---|
| AVHRR<br>search and rescue<br>sea surface currents<br>drifting buoys<br>search planning | Document is available to the U.S. public through the National Technical Information Service, Springfield, Virginia 22161 |

| 19. Security Classif. (of this report) | 20. SECURITY CLASSIF. (of this page) | 21. No. of Pages | 22. Price |
|---|---|---|---|
| UNCLASSIFIED | UNCLASSIFIED | | |

Form DOT F 1700.7 (8/72) Reproduction of form and completed page is authorized

# METRIC CONVERSION FACTORS

## Approximate Conversions to Metric Measures

| Symbol | When You Know | Multiply By | To Find | Symbol |
|---|---|---|---|---|
| | | **LENGTH** | | |
| in | inches | * 2.5 | centimeters | cm |
| ft | feet | 30 | centimeters | cm |
| yd | yards | 0.9 | meters | m |
| mi | miles | 1.6 | kilometers | km |
| | | **AREA** | | |
| $in^2$ | square inches | 6.5 | square centimeters | $cm^2$ |
| $ft^2$ | square feet | 0.09 | square meters | $m^2$ |
| $yd^2$ | square yards | 0.8 | square meters | $m^2$ |
| $mi^2$ | square miles | 2.6 | square kilometers | $km^2$ |
| | acres | 0.4 | hectares | ha |
| | | **MASS (WEIGHT)** | | |
| oz | ounces | 28 | grams | g |
| lb | pounds | 0.45 | kilograms | kg |
| | short tons (2000 lb) | 0.9 | tonnes | t |
| | | **VOLUME** | | |
| tsp | teaspoons | 5 | milliliters | ml |
| tbsp | tablespoons | 15 | milliliters | ml |
| fl oz | fluid ounces | 30 | milliliters | ml |
| c | cups | 0.24 | liters | l |
| pt | pints | 0.47 | liters | l |
| qt | quarts | 0.95 | liters | l |
| gal | gallons | 3.8 | liters | l |
| $ft^3$ | cubic feet | 0.03 | cubic meters | $m^3$ |
| $yd^3$ | cubic yards | 0.76 | cubic meters | $m^3$ |
| | | **TEMPERATURE (EXACT)** | | |
| °F | Fahrenheit temperature | 5/9 (after subtracting 32) | Celsius temperature | °C |

*1 in = 2.54 (exactly).


## Approximate Conversions from Metric Measures

| Symbol | When You Know | Multiply By | To Find | Symbol |
|---|---|---|---|---|
| | | **LENGTH** | | |
| mm | millimeters | 0.04 | inches | in |
| cm | centimeters | 0.4 | inches | in |
| m | meters | 3.3 | feet | ft |
| m | meters | 1.1 | yards | yd |
| km | kilometers | 0.6 | miles | mi |
| | | **AREA** | | |
| $cm^2$ | square centimeters | 0.16 | square inches | $in^2$ |
| $m^2$ | square meters | 1.2 | square yards | $yd^2$ |
| $km^2$ | square kilometers | 0.4 | square miles | $mi^2$ |
| ha | hectares (10,000 $m^2$) | 2.5 | acres | |
| | | **MASS (WEIGHT)** | | |
| g | grams | 0.035 | ounces | oz |
| kg | kilograms | 2.2 | pounds | lb |
| t | tonnes (1000 kg) | 1.1 | short tons | |
| | | **VOLUME** | | |
| ml | milliliters | 0.03 | fluid ounces | fl oz |
| l | liters | 0.125 | cups | c |
| l | liters | 2.1 | pints | pt |
| l | liters | 1.06 | quarts | qt |
| l | liters | 0.26 | gallons | gal |
| $m^3$ | cubic meters | 35 | cubic feet | $ft^3$ |
| $m^3$ | cubic meters | 1.3 | cubic yards | $yd^3$ |
| | | **TEMPERATURE (EXACT)** | | |
| °C | Celsius temperature | 9/5 (then add 32) | Fahrenheit temperature | °F |

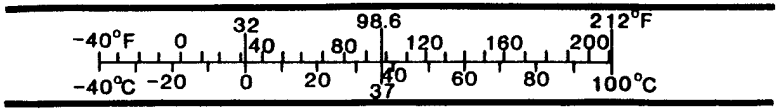

## TABLE OF CONTENTS

## LIST OF FIGURES

## LIST OF TABLES

## LIST OF ABBREVIATIONS AND ACRONYMS

| | |
|---|---|
| ACRSO | Atlantic Centre for Remote Sensing |
| ADCP | Acoustic Doppler Current Profilers |
| APT | Automatic Picture Transmission |
| ATSR | Along-Track Scanning Radiometer |
| AVHRR | Advanced Very High Resolution Radiometer |
| CANSARP | Canadian Search and Rescue Planning |
| CASP | Computer-Assisted Search Planning |
| CTD | Conductivity-Temperature-Depth |
| CZCS | Coastal Zone Color Scanner |
| DAT | Digital Archive Tape |
| DCC | Delaware Coastal Current |
| DDS | Digital Data Storage |
| DFO | (Canadian) Department of Fisheries and Oceans |
| EOS | Earth Observing System |
| FNMOC | Fleet Numerical Meteorology and Oceanography Center |
| GAC | Global Area Coverage |
| GCP | Ground Control Point |
| HF-GW | High Frequency-Ground Wave |
| HRPT | High Resolution Picture Transmission |
| IR | Infrared |
| ISARC | Improvement of Search and Rescue Capabilities |
| K | Kelvin |
| LAC | Local Area Coverage |
| LNA | Low Noise preAmplifier |
| MCSST | Multichannel Sea Surface Temperature |
| MEP | Marine Environment Protection |
| MSIC | Marine Science Information Center |
| MCC | Maximum Cross Correlation |
| NLSST | Nonlinear Sea Surface Temperature |
| NRL-SSC | Naval Research Laboratory at Stennis Space Center |
| SeaWiFS | Sea Viewing Wide Field-of-View Sensor |
| SIDSC | Satellite Imagery-Derived Surface Currents |
| SLDMD | Self-Locating Datum Marker Buoy |
| SST | Sea Surface Temperature |
| USCG | United States Coast Guard |

# 1.0 INTRODUCTION

Through satellite remote sensing a wide range of ocean parameters including ocean color, sea surface temperature (SST), height (with respect to the geoid), and surface roughness can be measured. Unlike ship or buoy measurements which can provide only a point sample, satellite sensors can measure the spatial variability over a vast region of the ocean surface (Robinson, 1985). Satellite observations have already contributed to our knowledge of the general circulation of the ocean, mesoscale eddies and upwelling, small-scale frontal systems, and internal and surface waves (Charnock, 1985). New satellite sensors are currently being designed and constructed to exploit and improve the observation methods already in use. It is imperative for oceanographers and U.S. Coast Guard (USCG) marine scientists to learn to utilize remotely sensed ocean data and to contribute to the development of new applications of space technologies to better serve Coast Guard mission requirements.

To this end, the Improvement of Search and Rescue Capabilities (ISARC) project of the USCG Research and Development Center, Groton, Connecticut, is evaluating the potential uses of satellite-derived imagery in Search and Rescue applications. Specifically, the objective of the project is to develop real-time techniques for deriving mesoscale oceanic currents from remotely sensed satellite imagery. This report focuses on AVHRR-derived sea surface currents.

## 1.1 BACKGROUND

A major difficulty with open ocean Search and Rescue missions is search area expansion resulting from drifting targets. From the instant of the last known position, the search area begins to expand and move in a highly variable manner dependent on environmental conditions and the accuracy with which these conditions can be estimated. The size and accurate location of the projected search area are directly related to the accuracy of the current data used to predict the drift. Presently, sea surface current information is obtained for the USCG Computer Assisted Search Planning (CASP) program from either the Fleet Numerical Meteorology and Oceanography Center (FNMOC) analysis model or a default database of historical current fields. However, accurate case-dependent data should always be used when available because minor differences in the estimated magnitude and direction of the sea surface current can greatly affect the predicted location of the target. Even well-established currents (for example, the Gulf Stream) can vary in location, direction, and intensity. The goal of the Satellite Imagery-Derived Surface Currents (SIDSC) project is the improvement of drift predictions for computerized search planning methods. These predictions will reduce search time and area and thereby utilize Coast Guard resources more efficiently in terms of cost and time. Most importantly a more rapid search will save lives and property.

Traditional methods for estimating target drift using case-dependent data have included current meters, drifting buoys, and direct temperature measurements. These methods, which all make use of point measurements, are time-consuming, costly, and can be inaccurate since it is impossible to determine how representative the measured water parcel is of the surrounding water. In time, even with an accurate datum (position of search target), the search area expands to the point where a prohibitive number of instruments would be necessary to obtain a picture of the regional surface current field. With no accurate datum, such as in the case of an overdue vessel, the initial area may be too great to be covered by deployed instruments. In addition, measurement of the currents in even a small area a long distance from shore can be extremely expensive because these methods all require on-site deployments. Therefore, the possibility of obtaining ocean surface velocities without having to make extensive field measurements prompted numerous attempts to estimate the velocity field from remotely sensed satellite images. Surface currents from satellite imagery can represent near real-time estimates of the currents over a large area, avoiding the aliasing problems inherent in traditional methods of current measurements.

The FNMOC current data are provided to the USCG on a $3^{\circ}$ x $3^{\circ}$ grid which means that the grid points are a nominal 180 nautical miles (300 km) apart. Mesoscale features, on the order of 50 to 300 km, may be too small to be resolved by FNMOC data (See Figure 1). This can result in gross and costly errors in predicting surface currents. For instance, Hurricane Andrew (1992) was too small to be resolved by the FNMOC data file. The Gulf Stream and its associated eddies are also examples of mesoscale features. Therefore, resolution of mesoscale features is important to the study of ocean dynamics, Search and Rescue operations, the fishery industry, and to many other diverse interests. Remotely sensed data have the potential to provide finer resolution than the product currently available from FNMOC. Since satellite infrared (IR) images often depict mesoscale features clearly (in the absence of cloud cover or excessive atmospheric water vapor), the use of Advanced Very High Resolution Radiometer (AVHRR) imagery for various oceanographic applications is expanding rapidly. ISARC anticipates that the currents derived from satellite images will provide worldwide data at the intermediate scale (5-20 km) between the FNMOC data (~300 km) and the Self-Locating Datum Marker Buoys (SLDMB) (<1 km). The FNMOC data will be used for oceanic scale search planning, the satellite imagery currents for regional planning, and the datum marker buoys for searches originating from a well-known datum. ISARC is currently modifying the modules within the CASP program so they can accommodate the SLDMB and the satellite-derived surface velocities to provide integrated localized real-time currents.

The potential applications of utilizing AVHRR-derived images were evaluated as part of a continuing effort to examine other forms of satellite ocean data, such as satellite altimetry and satellite-based radar, as those technologies and data become available. In June 1992, the ISARC project acquired a satellite receiving, display, analysis, and archiving system. The system, produced by Global Imaging of Solana Beach, California, tracks the NOAA TIROS-N series

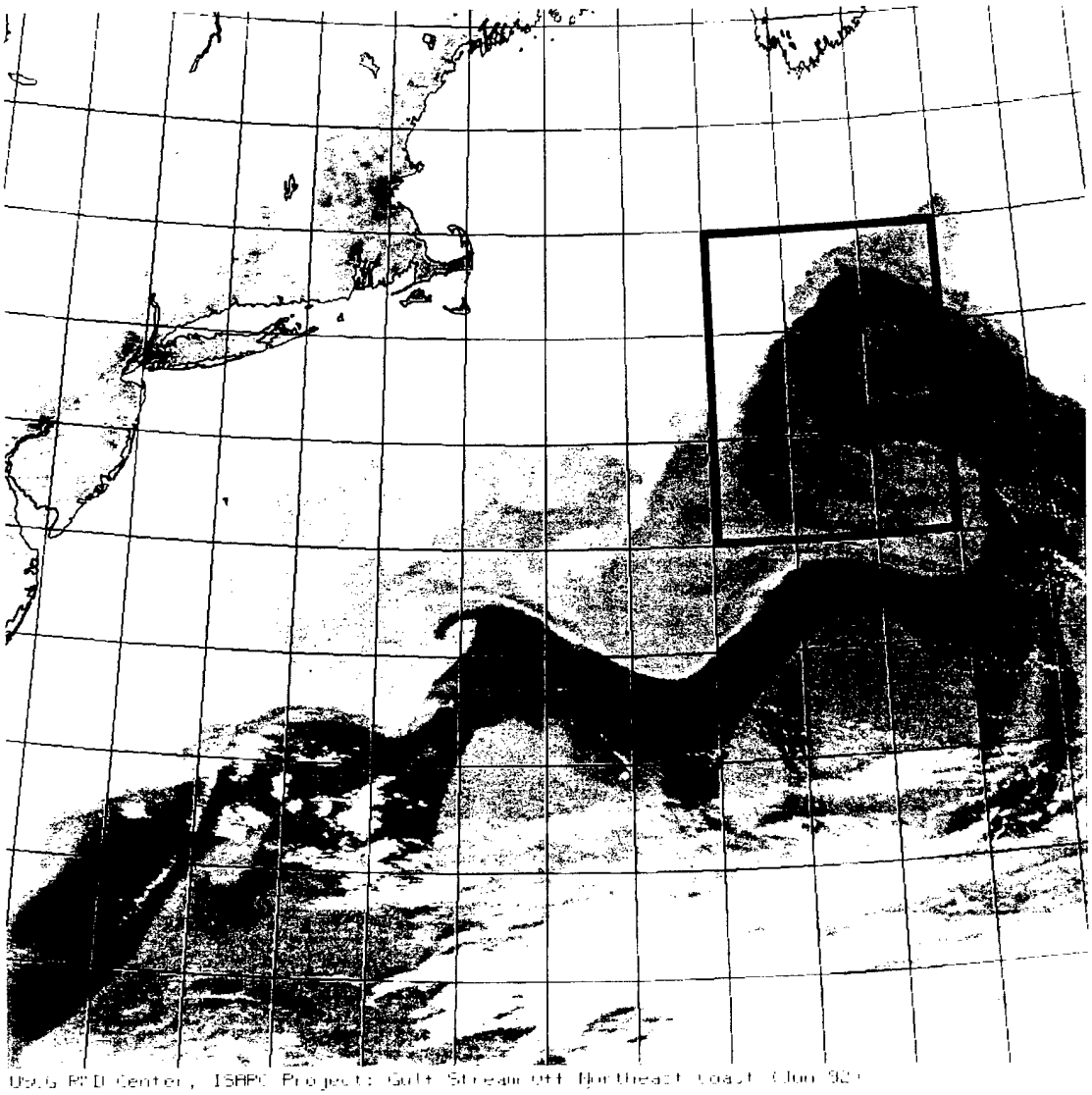

**Figure 1.** AVHRR Image of the Gulf Stream From June 1992. The box in the upper right corner denotes a 3° x 3° grid.

satellites, which are sun-synchronous and polar-orbiting. The satellites carry AVHRR, which is a five-channel multispectral scanner. Two channels are located in the reflective portion of the spectrum, and three are in the emitted thermal IR portion. The data from the three emitted thermal IR channels can be combined through empirically based equations to generate estimates of SST (Kidwell, 1991). Since the AVHRR sensor is an IR instrument, it measures the SST in only the upper 15 μm of the ocean. The SST measured by AVHRR has been found reasonably representative of the upper ocean when the local winds are between 5-10 m/s (Tokmakian et al., 1990).

Sea surface currents are estimated from the AVHRR-derived SST measurements by comparing a time-series sequence of images. The motion of thermal features between sequential images is determined. Knowing the distance the features have traveled and the time between the images, the surface currents can be estimated. The current vectors obtained provide a pattern of the sea surface circulation.

## 1.2 REPORT OUTLINE

This report presents the results of the SIDSC development, demonstration, and proof-of-concept program on the potential applications of satellite imagery for Coast Guard Search and Rescue missions. First, an overview of AVHRR and image processing will be presented. The techniques for estimating sea surface velocities from sequential AVHRR imagery will be described. Then, the three experiments performed to evaluate the operational feasibility and accuracy of the velocity estimates will be discussed. Recommendations are made for the design, implementation and integration of remotely sensed satellite-derived surface currents into the search planning process. Other Coast Guard applications are considered. The report concludes with a discussion of the future of AVHRR and other satellite remote sensors such as synthetic aperture radar, satellite altimetry and Along Track Scanning Radiometry (ATSR).

# 2.0 ADVANCED VERY HIGH RESOLUTION RADIOMETER

The only feasible method for obtaining a synoptic view of the ocean surface is through satellite remote sensing. AVHRR aboard the TIROS-N/NOAA series of weather satellites has been providing continuous IR images of SST patterns since 1972. AVHRR images have proved to be a valuable source of oceanographic data. The images have been used extensively to study mesoscale ocean features such as fronts and eddies. AVHRR provides radiometric data for day and night cloud mapping, SST, and other oceanographic and hydrologic applications.

AVHRR data are obtained from passive IR sensors aboard the polar-orbiting TIROS-N satellites. The five-channel AVHRR instrument measures radiances in the visible, near-infrared, and infrared regions of the electromagnetic spectrum (see Table 1). Channels 1 and 2 are in the visible region of the spectrum and can provide information on cloud cover, solar radiation during daylight, land-water boundaries, and snow and ice extent. When data from the two channels are compared, an indication of ice/snow melt inception is provided (Barnes and Smallwood, 1982). The last three channels measure in the near-infrared and the infrared regions of the electromagnetic spectrum. They provide information on cloud cover during nighttime and either single channel or multiple channel estimates of SST (Simpson, 1992a). Each channel is digitized to 1024 levels (i.e., 10 bit data) and calibrated from 0% to 100% reflectance for Channels 1 and 2 and from +/- 50° C for Channels 3, 4, and 5 (Lauritson et al., 1979, and updates). The absolute accuracy of the AVHRR-derived SST varies from .03 to 1° C; however, the relative accuracy is approximately 0.1° C which is adequate to identify most mesoscale thermal features (Robinson, 1985).

There are two operational NOAA-n series satellites in orbit. The orbits are spaced so one passes overhead between 6 and 10 a.m. local time. The other satellite passes over around 3 p.m. local time (Barnes and Smallwood, 1982). Each satellite provides daily coverage of the entire globe, acquiring data over a 2600 km swath width. This results in more overlapping of daily coverage at high latitudes.

AVHRR data can be acquired in real-time by Automatic Picture Transmission (APT) and High Resolution Picture Transmission (HRPT) receivers. However, these receivers can only obtain data from the AVHRR sensors while the satellite is within the receiving range of the APT or HRPT ground station. AVHRR data are also stored on board the satellite at a reduced resolution (4.4 km at nadir versus 1.1 km for HRPT) for subsequent downloading at Global Area Coverage (GAC) ground stations. AVHRR data are available in the four operational modes described below:

**Table 1.** Description of AVHRR Channels (adapted from Barnes and Smallwood, 1982).

| CHANNEL | WAVELENGTH (μm) | PRIMARY USE |
|---|---|---|
| 1 | 0.58 - 0.68 | Daytime cloud and surface mapping |
| 2 | 0.725 - 1.10 | Surface water delineation |
| 3 | 3.55 - 3.93 | SST, nighttime cloud mapping |
| 4 | 10.5 - 11.5 | SST, day/night cloud mapping |
| 5 | 11.5 - 12.5 | SST |

1) APT (Automatic Picture Transmission): direct readout to worldwide ground stations of the APT visible and IR data (4 km resolution): panoramic distortion is removed. Only two of the five available AVHRR channels are transmitted in the APT format. (Simpson, 1992a);
2) HRPT (High Resolution Picture Transmission): direct readout to worldwide ground stations of the HRPT data for all spectral channels (1.1 km resolution);
3) GAC (Global Area Coverage): global onboard recording of 4.4 km resolution data from all spectral channels for commanded readout/processing by the NOAA central computer facility; and
4) LAC (Local Area Coverage): onboard recording of data from selected portions of each orbit at 1.1 km resolution, of all spectral channels, for central processing (Barnes and Smallwood, 1982).

The major problem with AVHRR for application to oceanographic research is its inability to penetrate cloud cover. AVHRR was designed to monitor weather conditions, not oceanic processes. This shortcoming restricts the use of AVHRR SST measurements to times and areas that are relatively cloud-free.

## 2.1 SYSTEM CONFIGURATION

The basic elements of an AVHRR HRPT ground station are the antenna assembly, receiver, controller, and frame synchronizer (Figure 2). Alternative layouts are possible, and not all the units shown in Figure 2 are essential. The system used by the ISARC project consists of an earth station and a data and image processing module. The Telonics THRPT-4 Earth Station is a fully automated, portable 1698 and 1707 MHz (D-band) downlink reception station that automatically receives and synchronizes 665.4 Kb/s HRPT data. These elements are described below.

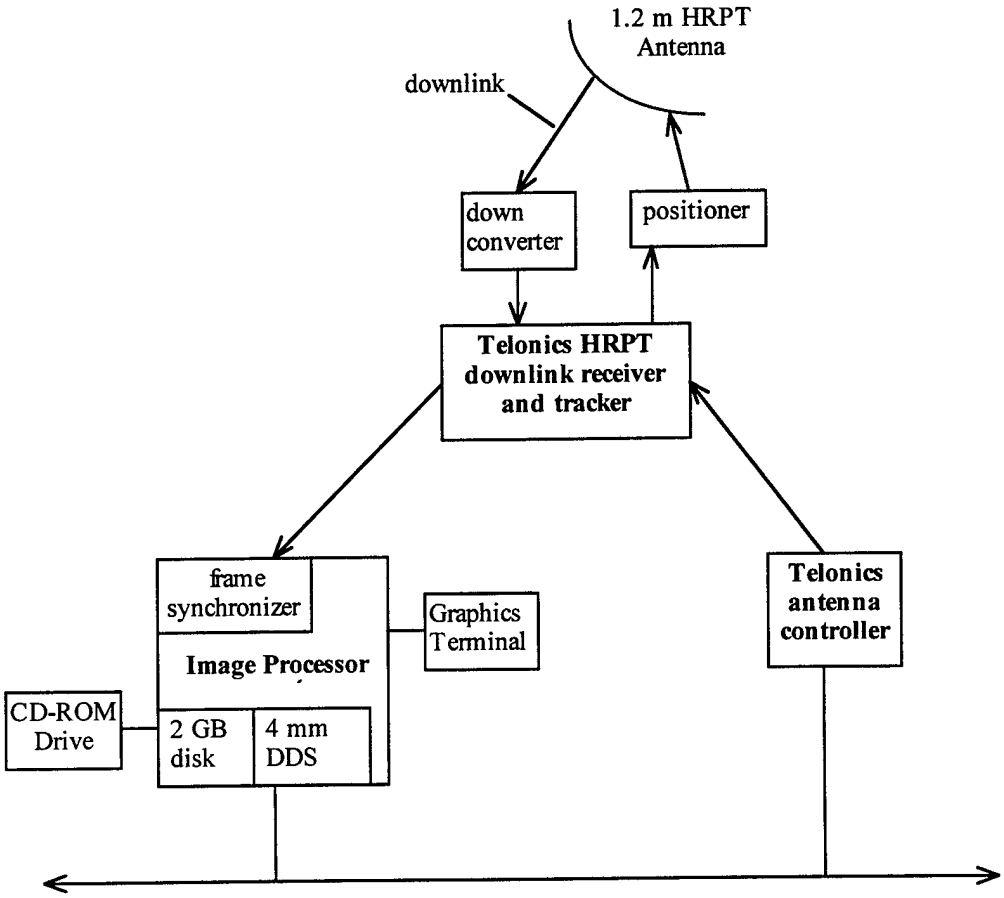


**Figure 2**. Schematic of ground control station.

## Antenna Assembly

The antenna system consists of interchangeable 1.0 m (portable for field work) and 1.2 m parabolic antennae, low noise temperature amplifiers, a cavity feed and wide temperature range down-converter. The assembly is manipulated by a $180^{o}$ elevation over $360^{o}$ azimuth positioner. The positioner is mounted on a pedestal of heavy aircraft aluminum and sealed for protection from the environment. The antenna system consists of a pedestal mounted positioner, a circularly polarized parabolic antenna, a high gain interdigital down-converter, and a Low Noise preAmplifier (LNA). The controller and positioner are capable of maintaining point resolution of $\leq 2°$. The antenna should be located so that a clear view of the horizon is available in all directions while avoiding long lead-in wires. The ISARC antenna is located on a nine-foot tower placed on a two-foot platform on the roof of the Research and Development Center. The distance between the antenna and the remote sensing laboratory where the rest of the data acquisition module is located is approximately 20 m.

## Receiver

The receiving subsystem is a remote controlled down-link Intermediate Frequency unit designed specifically for the reception of HRPT downlink data. The Low Noise preAmplifier and down-converter mounted on the antenna assembly are companion components of the receiver subsystem.

## Controller

The antenna controller is an integral part of the earth station. The controller provides tracking information to the antenna. It is also used to acquire orbital elements via an electronic bulletin board. The computer offers an LCD display of continuous orbital subtrack for help in planning data acquisition as well as a numerical display of the earth coordinates of the orbital subtrack. Computer interaction with the receiver for automatic frequency selection is accomplished through the antenna controller unit. The controller receives all control interface signals for the receiver from the ephemeris computer.

## Frame Synchronizer

Before the data received can be manipulated by data processing systems, the serial bit stream from the bit conditioner must be sliced into words of the correct length, or into groups of words. AVHRR data words are 10 bit. The frame synchronizer must correctly identify the start of each word or the data will be rendered useless.

**Data Archiving Unit**

This unit consists of a 2-Gbyte Digital Data Storage (DDS) drive, commonly known as a DAT (Digital Archive Tape) drive.

**Data Acquisition and Image Processing Module**

This module consists of an HP 715/100 Series workstation with 32 Mbyte RAM and 2 Gbyte disk capacity, and a 1280 x 1024 bit 20 inch color monitor with 8 graphics planes and 4 overlay planes.

# 3.0 DATA PROCESSING

Remotely sensed satellite data must be preprocessed before meaningful analysis can be performed. The raw telemetry bit stream transmitted to the ground stations has little resemblance to the maps of SST. Several preliminary processing steps are required to produce SST maps, which then serve as the basis for all other AVHRR-derived operational products (Simpson, 1992a). Data processing of all satellite measurements consists of four general stages: sensor calibration, positional registration, atmospheric correction and geophysical calibration. The approach to the calibration and correction varies greatly with different types of sensors (Robinson, 1985). Figure 3 is a flow chart of the recommended sequence of preprocessing steps for AVHRR data for oceanic search planning. Sensor calibration is performed to correct for sensor drift. Sensor drift can create problems when analyzing images received several months apart. Sensor calibration is performed before the satellite's launch and during the satellite's lifetime by space technologists. The data user is dependent upon the technologists to perform precise calibrations prior to launch, to conduct as many in-flight calibration procedures as possible, and to publish the details (including modifications and updates) of the calibration procedures. While it is essential for the AVHRR user to be aware of errors caused by sensor drift, the user has no choice but to accept the calibration data (Robinson, 1985).

Positional registration is the process of identifying the geographical location of the sensor data on a map projection. The adjustment of the image to make it conform to a map base is called the navigation of the image. Atmospheric corrections must also be performed to reduce the effects of having to measure the sea surface through another medium, namely the atmosphere. Significant processing must be performed to identify clouds and fog and to reduce the effects of gas molecules, water vapor, aerosols and suspended particles of dust. Geophysical calibration is the conversion of the measurement of radiances into useful parameters such as SST.

Image processing refers to procedures performed on the image data to enhance properties of interest, to assist in interpreting the data, or to extract useful information (Robinson, 1985). Image processing algorithms can produce artifacts that may be misinterpreted as oceanographic features; however, if the image data contain no information on a particular property, no amount of image processing can produce it. Yet by using image processing techniques such as smoothing and enhancing, it is possible to generate pseudo-patterns that may appear to represent oceanographic features. To avoid this error, the user should consider sensor resolution and calibration in terms of oceanographic parameters while processing satellite images (Robinson, 1985).

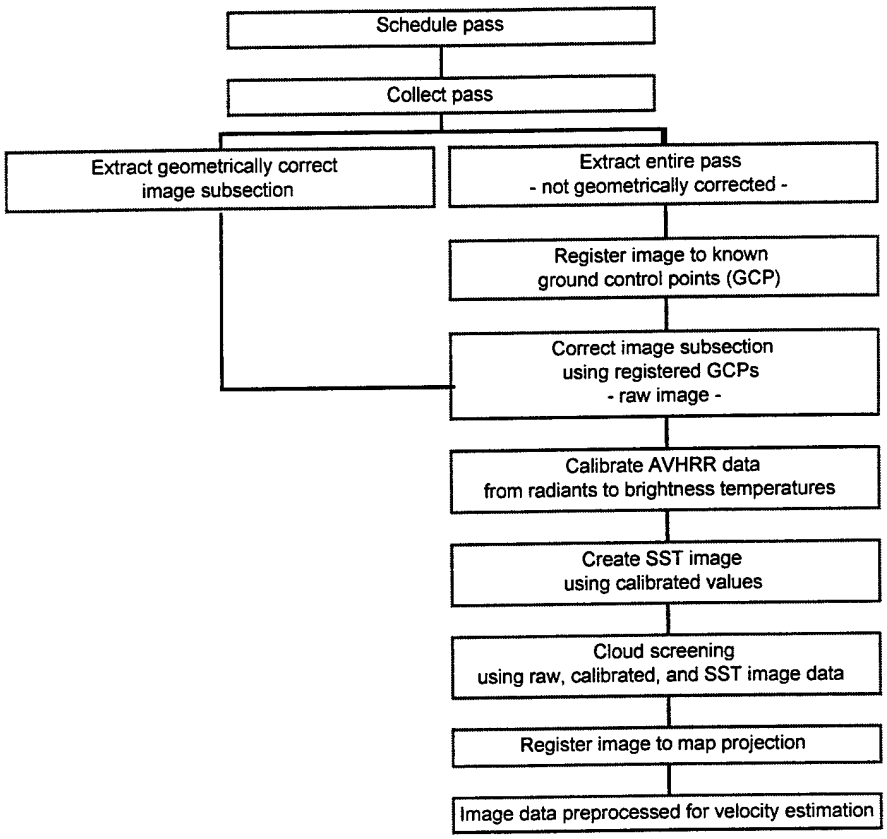


**Figure 3.** Sequence of preprocessing steps for AVHRR images for sea surface current estimation.

## 3.1 GEOMETRIC CORRECTION

The first step in processing a remotely sensed image is to use a geometric correction procedure to correct for distortions from oblique viewing over a wide range of satellite viewing angles. Geometric correction uses the orbital and sensor geometry data contained in the header of the data stream from the satellite. The image is initially registered using an earth location file created from the ephemeris and geometric-correction programs. This theoretical rectification transformation removes the major earth curvature and oblique viewing distortions by "stretching" each scan line to allow for the distortion caused by oblique viewing angles and then mapping the stretched scan lines onto a base map by identifying the latitude and longitude of each pixel (Robinson, 1985). The accuracy of this technique is limited by the time accuracy of data transmission and by random displacement of the satellite from its theoretically predicted satellite orbit.

The second step is to correct for the random displacements of the satellite and to eliminate satellite clock errors by using known reference locations (ground control points (GCP)), and to register these changes on the base map. For a scanned image, such as AVHRR, it is not sufficient to register just one GCP because the image may be rotated and distorted as well as translated laterally from its theoretically expected position. To correct for the distortions, GCPs on the image are identified and their pixel locations are noted. The pixel coordinates are then associated with the pixel locations of the GCPs on the base map projection of the imaged area. Using a generalized warping algorithm, the pixel locations of the GCPs on the image are fitted to the pixel locations of the GCPs on the base map. The rest of the image is stretched and rotated unevenly across its surface. The accuracy of registration of each pixel depends on the accuracy of identification of GCPs and on their uniform distribution throughout the scene[1] (Robinson, 1985). At best, the image can be corrected to within approximately one pixel, 1.08 km square. The estimation of sea surface velocities from sequential images requires a high degree of navigational accuracy. The Global Imaging navigational algorithm was insufficiently accurate for comparison of images. A navigation algorithm was needed that was not only accurate, but also easy to learn, uncomplicated and time efficient. The SIDSC project acquired a navigation algorithm that fulfills these requirements from the Naval Research Laboratory at Stennis Space Center (NRL-SSC). The algorithm was integrated into the SIDSC system and evaluated for suitability to search planning objectives. The navigation procedure is very time-consuming, as is any generalized warping process; however, by using a combination of ephemeris data and GCPs to register the image, time and labor are reduced while location accuracy is increased.

### 3.2 DATA EXTRACTION

A subset of the image data centered over an area of interest is extracted from the satellite data stream during a pass and stored as a two-dimensional data array.

### 3.3 CALIBRATION

The third step in processing an AVHRR image is the conversion of each channel from brightness counts to geophysical units (i.e., percent albedo for Channels 1 and 2, and degrees Celsius for Channels 3, 4, and 5). Using the AVHRR calibration data and assuming the ocean surface to be a black body, the black body relationship between temperature and radiance is applied to convert the radiometer readings to degrees Celsius (Kelly, 1983). The calibration relationships are published in NOAA Technical Memorandum NESS 107 (Lauritson et al., 1979

[1]The number and location of GCPs necessary for accurate navigation for oceanic search planning is discussed in Sumner (1993).

and updates). The Global Imaging software converts the raw counts for each AVHRR channel into radiance values or temperature depending on user specifications. From the user's perspective the calibration of the AVHRR data is quick and uncomplicated.

## 3.4 SEA SURFACE TEMPERATURE CONVERSION

The next step in the processing of AVHRR data is to convert the calibrated values into a representation of the SST. The SST is frequently calculated by a linear combination of the radiances from two (Channels 4 and 5) or three (Channels 3, 4, and 5) channels of the AVHRR. Because the atmospheric contributions are different at night from during the day (there is no reflected solar radiation at night), different algorithms must be used to process daytime and nighttime images. A nonlinear expression is available, but it would only improve the SST about 0.1° C. For search planning requirements, a linear multichannel SST (MCSST) conversion is sufficient. However, if requirements change, it is possible to alter the MCSST to a nonlinear SST (NLSST).

The MCSST algorithms are based on the following equations developed by McClain et al., (1985):

$$T_{45}=C_0 T_4 - C_1 T_5 - C_2 \qquad 1$$

for a two-channel MCSST and

$$T_{345}=C_3 T_4 + C_4 (T_3 - T_5) - C_5 \qquad 2$$

for a three-channel MCSST, where $T_3$, $T_4$, and $T_5$ are brightness temperatures measured by the AVHRR Channels 3, 4, and 5 wavelengths, respectively, and $T_{45}$ and $T_{345}$ are the SSTs. The calibration parameters $C_n$ are assumed to be constant in the MCSST algorithms. Equations (1) and (2) are widely accepted and suggest that SST is basically proportional to the brightness temperature measured from space, but should also include a term for correction of atmospheric effects. The Global Imaging MCSST algorithms have been modified to include a path length correction. This corrects for errors in SST resulting from the increased path length of the signal to the satellite at the edges of the image compared with the path length at nadir.

The performance of the MCSST algorithms is dependent on the coefficients. These are usually determined by regression of satellite data with synchronous in situ data. To develop an accurate algorithm it is necessary to regress a large number of satellite data with in situ data so that the algorithm can be used for different locations and for different seasons. However, this approach is difficult for the following reasons. First, there are limited qualified in situ data available to match with the satellite data. A set of coefficients that is good for one area or one season can give poor performance for other areas or other seasons. Additionally, when an

exceptional atmospheric condition is encountered, such as when a volcanic eruption produces unusually high levels of stratospheric dust in a low-latitude belt around the world, the coefficients will be incorrect and must be re-evaluated (Robinson, 1985). Secondly, most of the in situ data obtained by conventional ship- or buoy-mounted thermometers are measurements of "bulk" SST which represents the sea temperatures in the range 0.5-3.0 m under the surface, whereas the satellite measurements represent "skin" temperatures in the top few micrometers. The regression analysis does not account for any difference between the bulk and skin temperatures (Yu and Barton, 1994). The difference between the bulk and skin temperature is greatest on sunny afternoons on relatively calm days when radiometric measurements of SST may differ by up to a degree from the bulk SST as measured from a ship or buoy. At night the diurnal thermocline is destroyed because of wind-stirring and surface heat losses to the atmosphere lacking any incoming solar radiation (Robinson, 1985).

## 3.5 CLOUD SCREENING

The radiometry signal from clouds is so that large cloud contamination represents the most significant source of error in SST measurements derived from AVHRR data (Gallaudet and Simpson, 1991). Therefore, the quality of the SST estimates is critically dependent upon the accurate identification and removal of the cloud-contaminated pixels from the image.

Cloud identification is a difficult problem. Clouds are usually colder than the ocean surface and their temperature variance is an order of magnitude larger than that of the ocean (Kelly, 1983). Low clouds and fog can be particularly difficult to distinguish from cold fronts. Clouds that are thin or smaller than the sensor's field of view are hard to detect. The effect of clouds on SST measurements is dependent upon the type of cloud present. Large, dense clouds completely obscure the ocean temperature signal beneath them. If the clouds are dense, but scattered, oceanic features may be visible between the cloud-contaminated pixels. If the clouds are smaller than the sensor resolution (approximately 1 $km^2$), they will not usually be visible in the image (Kelly, 1983). However, these clouds lower the apparent SST so the errors in the SST estimation are not obvious.

Cloud screening is a process in which pixels containing clouds are identified and masked while the remaining pixels are retained for analysis. For analyses requiring only a few images, manual cloud screening may be acceptable, but for operational use, automated cloud identification and masking is crucial. A variety of techniques for identifying and removing cloud-contaminated pixels is available. These range from simple radiance thresholds to complicated procedures

involving artificial intelligence techniques. Cloud screening algorithms have shown varying degrees of success, the effectiveness of the particular method used being critically dependent upon cloud type (Simpson and Humphrey, 1990). Dealing with contamination from cirrus clouds, for example, has been a major deficiency of cloud screening algorithms. A single cloud identification and removal technique is usually insufficient. Daytime and nighttime passes frequently require different techniques. The accuracy of some techniques exhibits geographic dependency because of variations in meteorological and oceanographic conditions. Therefore, many analysts are combining a series of techniques (Gallegos et al., 1992). Cloud screening algorithms are still unable to correctly identify all cloud-contaminated pixels, frequently requiring AVHRR images that have been processed using automated cloud screening techniques to be processed manually to identify cloud-contaminated pixels not identified by the automated technique.

The Global Imaging cloud screening techniques are based on a simple radiance threshold technique. This is too primitive for SIDSC requirements because it may eliminate valuable data from the image or interpret regions of high oceanic gradient as cloud. This treatment of gradients is particularly a problem for surface velocity estimation because of the need to identify thermal fronts (Simpson, 1992a). A study was necessary to determine which currently available cloud screening algorithm would best suit search planning needs in terms of ease of use, automation, and speed. Operational search planning requires a cloud screening algorithm that can accurately and efficiently identify and mask cloud-contaminated pixels from real-time AVHRR images. The Naval Research Laboratory at Stennis Space Center (NRL-SSC) had similar requirements for their cloud screening algorithm. After deciding that none of the currently available algorithms satisfied their requirements, NRL-SSC developed an automated technique to identify and mask clouds from AVHRR daytime and nighttime images.

The NRL-SSC method uses a series of tests to identify the cloud-contaminated pixels (Gallegos et al., 1992). The clouds are identified by their spectral and textural features. The NRL-SSC algorithm is valid over a wide range of latitudes and allows processing of data along the entire swath of the AVHRR image, including areas of sunglint. The algorithm was found to perform well in comparison with other operational and experimental cloud masks and with cloud masks produced visually by an experienced operator (Gallegos et al., 1992). Since the NRL-SSC algorithm was developed in response to requirements similar to the Search and Rescue program in terms of accuracy, time efficiency and geographic independence, it was selected as the cloud screening algorithm, currently available, that is best suited to our needs. The source code was not available from NRL-SSC, so a version of the software, based on the NRL-SSC algorithm, developed by the Atlantic Centre for Remote Sensing of the Oceans (ACRSO) was acquired. Upon installation and testing, this algorithm did not completely fulfill SIDSC requirements. The software was modified to correct errors in the algorithm and to improve the cloud screening performance for nighttime passes. Based on a cloud-detection algorithm proposed by Kubota (1992), the ACRSO algorithm was revised to incorporate two-dimensional histograms for

identifying cloud-contaminated pixels as opposed to using a simple radiance threshold. A key attribute of the revised version is the inclusion of a recovery function. To reduce the possibility of masking cloud-free pixels erroneously, the recovery function allows a pixel to be recovered even if one of the cloud detection tests indicates the pixel may contain clouds.

No one cloud screening algorithm has been found to differentiate consistently and accurately between clouds and ocean. The technique developed by SIDSC incorporates several cloud-detection tests, but still requires a degree of manual processing for identification of low clouds and fog. It is unlikely that pixels contaminated by very small clouds will ever be eliminated, even by manual methods, but the errors should be within acceptable bounds (Robinson, 1985).

## 3.6 REGISTER IMAGE TO MAP PROJECTION

The final preprocessing step is to register the image to a given map projection (for example, Mercator, polar stereographic) by identifying the correct latitude and longitude for each pixel in the image.

# 4.0 SEA SURFACE VELOCITY ESTIMATION

The availability of high resolution satellite images of IR SSTs led to an interest in the feasibility of computing remotely sensed sea surface currents. By comparing sequential AVHRR images, the movement of SST features can be detected from which the speed and direction of surface currents are inferred (Kelly and Strub, 1992). It has been shown by Kelly (1983) that SST patterns are consistent with current measurements from Lagrangian drifters. Methods for estimating surface currents from satellite imagery fall into two categories: those that follow the movement of the surface features and those that use the heat equation (which describes the balance of temperature fluxes at the ocean surface) and the estimated SST. The former are called feature tracking methods. They do not make use of the actual SST and thus are less sensitive to errors in converting IR radiance values to temperature. Inversion of the heat equation requires a correction for atmospheric conditions and satellite viewing angle, but is better suited to the inclusion of data from additional sources such as drifting buoys and numerical models. The two techniques were evaluated to determine which method was better suited to fulfill the operational requirements of the Search and Rescue program.

## 4.1 FEATURE TRACKING

Feature tracking is a subjective, interactive technique in which an operator uses an interactive system to display sequential satellite images. The main approach of determining flow velocities from IR and visible imagery using feature tracking is to follow distinct thermal or color features through sequential images. Generally, two images, recorded 6-24 hours apart, are used. The operator flickers back and forth between sequential images to select small features visible in both images and to locate their positions. The calculated displacement over the time separation between images gives the local flow velocity estimate. The accuracy of feature tracking is affected greatly by the type and stability of features selected and the positioning accuracy of the imagery. Svejkovsky (1988) reasoned that feature tracking is not valid in regions where the SST patterns change rapidly, such as areas of strong tidal flows or during periods of strong wind mixing. An inherent weakness in this technique is that it is highly subjective. Selection and tracking of the features vary with operator, consequently the magnitude and direction of the velocity vectors determined by different operators from the same image pair, may differ. Additionally, detectable features are unlikely to have a high density in the region of interest so that many velocity values will not be calculated. Therefore, many investigators (for example, Holland and Yan, 1992; Emery et al., 1986, Tokmakian et al., 1990) have developed computational procedures, such as maximum cross-correlation (MCC), to calculate objectively surface velocities from sequential satellite image pairs. Most of these procedures are based on the pioneering work of Emery et al. (1986), who developed an automated computational procedure for estimating the displacements of small regions of SST patterns between sequential

AVHRR images. In this procedure the displacement of a feature is identified by the cross-correlation of a small subregion (roughly 18 x 18 km) of the initial image with a region from the subsequent image, searching for the location in the second image that gives the maximum cross-correlation coefficient. The velocity vector is computed from the displacement of the subregion and the time lag between the image pairs. The displacement is assumed to be the distance between the initial central location of the subregion and the center of the subregion in the second image with the maximum cross correlation.

## 4.2 HEAT INVERSION

Unlike feature tracking methods, inversion of the heat equation is an objective procedure for estimating sea surface currents from satellite imagery (Kelly, 1989). The surface temperature fluctuations are balanced by sea surface velocities using the temperature conservation equation:

$$T_t + uT_x + vT_y = S(x,y) + m(x,y) \qquad 3$$

where $T_t$ is the temporal derivative of SST; u,v are the horizontal velocity components; and $T_x$, $T_y$ are the horizontal gradients of SST. The right-hand side of the heat equation represents SST fluctuations that are due to residual measurement errors, surface heat fluxes, mixing, and vertical advection. The large spatial scale residual, S, is presumably not due to advection. The smaller-scale residual, m, is an error term that is minimized in the inversion (Kelly and Strub, 1992).

The null space for the heat inversion equation (3) contains velocity vectors that are parallel to isotherms and any velocity in regions of negligible SST gradients, because these velocities do not cause temporal changes in the SST (Kelly and Strub, 1992). Without any constraint on the solutions to the heat inversion equation, only the cross-isotherm velocity component will be generated. With the addition of a constraint on the solution, the inversion equation provides plausible total velocity fields (Kelly, 1989). Kelly and Strub (1992) investigated the effects of constraining the heat inversion by minimizing divergence, kinetic energy and relative vorticity. They found that minimizing divergence produced solutions that most closely resembled the in situ data. Minimizing the divergence forces SST changes in the model to be made by advection of thermal features rather than by convergence or divergence (Kelly, 1989). The importance of the divergence relative to the fit of the velocity solutions to the heat equation (3) is determined by varying a weighting factor, $\alpha$ (Kelly and Strub, 1992). The weighting factor is varied over a wide range to find the solution that produces the most realistic velocity field. Kelly and Strub (1992) computed seven solutions, with the parameter $\alpha$ varying from 0.005 to 0.32. The optimum value of $\alpha$ was determined subjectively to give large jet velocities without large divergences or large

velocities without large divergences or large velocities near the edges of the image (Kelly and Strub, 1992). The subjective determination of the weighting parameter $\alpha$ on the divergence represents the most significant disadvantage of using the heat inversion technique operationally.

## 4.3 COMPARISON OF VELOCITY ESTIMATION TECHNIQUES

In their comparison of the heat inversion technique and the MCC method, Kelly and Strub (1992) determined that both methods could produce near real-time representations of energetic flow features. The flow fields estimated from AVHRR imagery by both methods were in qualitative agreement with the velocities measured by Acoustic Doppler Current Profilers (ADCP) and drifter measurements on scales greater than 50-100 km. Both methods consistently underestimated the magnitude of the velocities measured in situ at 20 m depth. Kelly and Strub (1992) surmise that this underestimation of the velocities is inherent in the AVHRR data, rather than a limitation of the methods. The directional differences between the current derived from AVHRR data and those from in situ data were comparable to the differences between the ADCP and the drifter data. Kelly and Strub (1992) suggest that the heat inversion and MCC methods are equivalent in that the small-scale features cross-correlated in the MCC method must be the same features used to produce the SST differences in the inversion of the heat equation. Despite the similarity in the comparison statistics of the two methods with the in situ data, the AVHRR-derived fields differed from each other nearly as much as they differed from the in situ data.

Since the two techniques may be considered equally accurate, the techniques were evaluated as to which technique is better suited to fulfill the unique requirements of the Coast Guard operational Search and Rescue program. The overriding difference between the two techniques is that the feature tracking/MCC methods estimate the velocity by following the motion of small features assumed to be associated with water parcels, passively advected by the flow, while the heat inversion technique requires the velocity field to satisfy certain physics. For operational use, several potential problems must be considered: generation of an incoherent velocity field, estimation of the cross-isotherm velocity rather than the total velocity field, operator dependence, optimum time separation between image pairs, requirement for accurate SST data, and ease of incorporation of other data sources. These factors are discussed below.

## Incoherent Velocity Field

Velocity vectors estimated from feature tracking methods suffer from directional ambiguity, resulting in an incoherent velocity field (Simpson, 1992b). There are two ways to correct for this: either an operator selectively removes the erroneous velocity vectors (which, if all the incorrect vectors are systematically removed, would result in a loss of 60-70% of the data) or high-pass filtering is performed. Simpson is developing a technique that makes use of the nearest neighbor for directionality and then filters the resulting velocity field to overcome the directional ambiguity. Although this may be perceived to be a disadvantage to the feature tracking technique, filtering is analogous to removing the large scale residual term in the heat equation (Kelly and Strub, 1992).

## Cross-Isotherm Versus Total Velocity Field Estimation

A major disadvantage of feature tracking methods is that they detect the motion of thermal fronts and identify the motion as a current. When such fronts are associated with geostrophic currents, the surface currents should move along rather than across the thermal fields. Thus, the predominant surface currents along the features will be undetected by feature tracking methods, whether operator dependent or automated, resulting in erroneous estimates of the surface currents. Emery et al. (1986) observed that the SST features frequently have small-scale cross-frontal structures that move along the temperature gradient. The MCC method detects the motion of these small temperature filaments as velocities parallel to surface temperature contours. However, when SST signatures of wave motion are present, it may be difficult to distinguish between the sought-after advective motion, and wave-related phase velocities (Breaker et al., 1992). The solution of the heat equation, on the other hand, can give plausible velocity vectors parallel to the isotherms as well as the cross-isotherm velocity component, resulting in an estimate of the total velocity field. Since the predominant surface currents are along rather than across the isotherms, this is a significant advantage. The major difference between the two types of techniques is that feature tracking methods are based on recognition of color or thermal patterns without regard to the physics of the sea surface. Inversion of the heat equation is based on theoretical interpretation of the physics of the sea surface. Although it may seem intuitively preferable to require the velocity field to satisfy certain physics, Kelly and Strub (1992) suggest that the two methods are statistically equivalent.

## Operator Dependence

Although a completely automated SIDSC system is unlikely (Strub, 1992; Kelly, 1992), it is desirable to automate as many procedures as is feasible. Not only is a semi-automated system more objective, it also reduces operator training and experience requirements, and it is more efficient in terms of time and human resources during Search and Rescue operations. Estimating surface velocities by feature tracking is highly operator dependent and time extensive. Utilizing an MCC algorithm would lessen this shortcoming, but it would never be as automated as estimating velocities by inversion of the heat equation.

## Optimum Time Separation

There is an optimal time separation between image pairs. If the separation is too large, the image features may be difficult to follow from one image to the next. If the feature moves beyond the borders of the initial image during the time interval, the size of the image subset can be increased so the feature will be located in the subsequent image subregion, with a resulting increase in computation time. Features may also change too much between image pairs with long time separations to correlate or they may simply disappear. If the temporal separation between image pairs is too small, the movement of the water parcel may be small compared with measurement errors, resulting in large errors in the computed current field. The inversion of the heat equation works better with longer time separation between images (approximately 12 hours) while the MCC method has a shorter optimal temporal separation (4-6 hours) (Kelly and Strub, 1992). The longer separation of the heat inversion technique allows more potential passes from which to select images pairs. Less desirable images due to viewing angle, cloud cover, or lack of identifiable features would be less of a problem than with feature tracking methods. The shorter optimum separation of the feature tracking techniques would be an advantage when the area of interest is only clear for a short time due to changes in cloud cover. The feature tracking method may also be more successful when SST gradients are weak or when the SST cannot be calibrated correctly.

## SST Accuracy

An additional advantage to the feature tracking algorithms is that absolute SST is not required. Absolute SST is estimated by relating energy emitted at the ocean surface and absorbed by atmospheric water vapor to differences in energy detected by the satellite at several IR wavelengths. As discussed previously, satellite-derived SST accuracy is limited by sensor design and calibration, algorithms to correct for environmental factors such as sunglint, water vapor and aerosol absorption, data processing procedures, and local variations in air-sea interactions. Feature tracking performs equally well on relative SST or thermal or color gradients, thus

eliminating the errors inherent in converting IR radiance values to temperature. In contrast, successful implementation of the heat inversion technique requires accurate absolute SST.

**Incorporation of Additional Data**

An advantage to the heat inversion technique is the ease with which other sources of velocity data can be incorporated into the results. An element of the Self-Locating Datum Marker Buoys (SLDMB) development program is the integration of SLDMB drift data with model outputs and satellite-derived velocities to provide localized real-time currents. State-of-the-art environmental files are currently being integrated with the SLDMB drift data into the CASP system. The synthesis of this model and SLDMB data with the AVHRR-derived currents will be useful in constraining the AVHRR-derived current fields, and may significantly improve the derived velocity fields. A goal of the SIDSC project is the inclusion of satellite altimeter data in the velocity field estimates. (A satellite altimeter, a pencil-beam microwave radar that measures the distance between the satellite and the earth, can yield measurements of sea surface roughness from which the geostrophic current, average wave height and wind speed can be estimated.) The heat inversion technique is designed to include these other sources of data with an ease that is not feasible with the feature tracking methods.

Given the advantages and disadvantages of the two methods, it would seem plausible that a technique that could combine the two types of procedures would be optimum. Kelly and Strub (1992) found when they combined the MCC and heat inversion techniques that the combined solution offered no obvious gain in information or accuracy.

A disadvantage of both the feature tracking and heat inversion methods is that they are based on the assumption that only horizontal advection affects SST. This neglects the change in SST caused by other processes, such as vertical advection (upwelling and downwelling), local heating (or cooling) and mixing (both horizontal and vertical, although it is unlikely that within 24 hours diffusion will alter the SST (Emery et al., 1986)). It is reassuring that Kelly and Strub (1992) found that both methods can produce nearly instantaneous pictures of the surface current field that agree qualitatively with in situ measurements from ADCP and drifting buoys.

Neither technique is clearly preferable; however, two features in particular made the heat inversion technique more attractive for the Search and Rescue program. First, other sources of data can be incorporated easily into the velocity field solution. Secondly, the heat inversion technique is more objective and is less dependent upon operator experience and input.

# 5.0 EXPERIMENTS

SIDSC participated in three experiments to evaluate the potential of AVHRR to acquire useful data for oceanic searches in an operational setting. The data collected during the experiments were used to perform a comparative analysis of surface currents measured by satellite-tracked drifting buoys and those estimated by the heat inversion technique.

## 5.1 CAPE RACE

The ISARC project participated in a joint experiment with the Canadian Coast Guard off the coast of Cape Race, St. John's, Newfoundland. The objective of the experiment was to compare three distinct methods of deriving sea surface currents: drifting buoys, High Frequency-Ground Wave (HF-GW) radar and AVHRR images. The methods tested vary considerably in complexity, area of coverage, accuracy and cost. Two Argos drifter buoys provided by the Canadian Department of Fisheries and Oceans (DFO) were deployed. The drifter tracks recorded by DFO were compared with estimates of sea surface current obtained from a single HF-GW radar. ISARC provided remotely sensed AVHRR images acquired by the satellite receiving station at the R & D Center. The currents derived from these different methods of remote sensing were compared with existing Canadian Search and Rescue Planning (CANSARP) drift models.

### AVHRR Data

The joint US/Canadian Coast Guard experiment occurred off the coast of Cape Race, St. John's, Newfoundland, from 19 October to 1 December 1992 (Julian Days 293 - 336). The AVHRR images were registered to a grid that extends from approximately 40°30'N to 48°20'N and from 48°W to 59°W. An image from 19 October 1992 is shown is Figure 4. Clouds are represented by dark grey and the land is masked to black. This is the most cloud-free image collected during the experiment. As expected, cloud cover and fog greatly reduced the SST data. Figure 5 shows the total number of passes captured each week during the experiment. For the Cape Race Experiment, any image that had even a small cloud-free section was considered to have scattered clouds. Of the 119 passes captured, only 37, or about 31%, had some cloud-free areas. The optimum time separation between satellite images is 12 hours for the heat inversion technique. There are two constraints on the potential number of usable image pairs: the time separation between images and the extent and location of clouds. The image pairs that satisfy the time separation constraint (i.e., are separated in time between 6 and 24 hours) are shown in Figure 6. For a given image there may be more than one image pair that fits the time constraint.

**Figure 4.** SST off Cape Race, Newfoundland, from the AVHRR image on 19 October 1992, 22 Z. Land is masked to black. Lighter gray shades correspond to cooler temperatures.

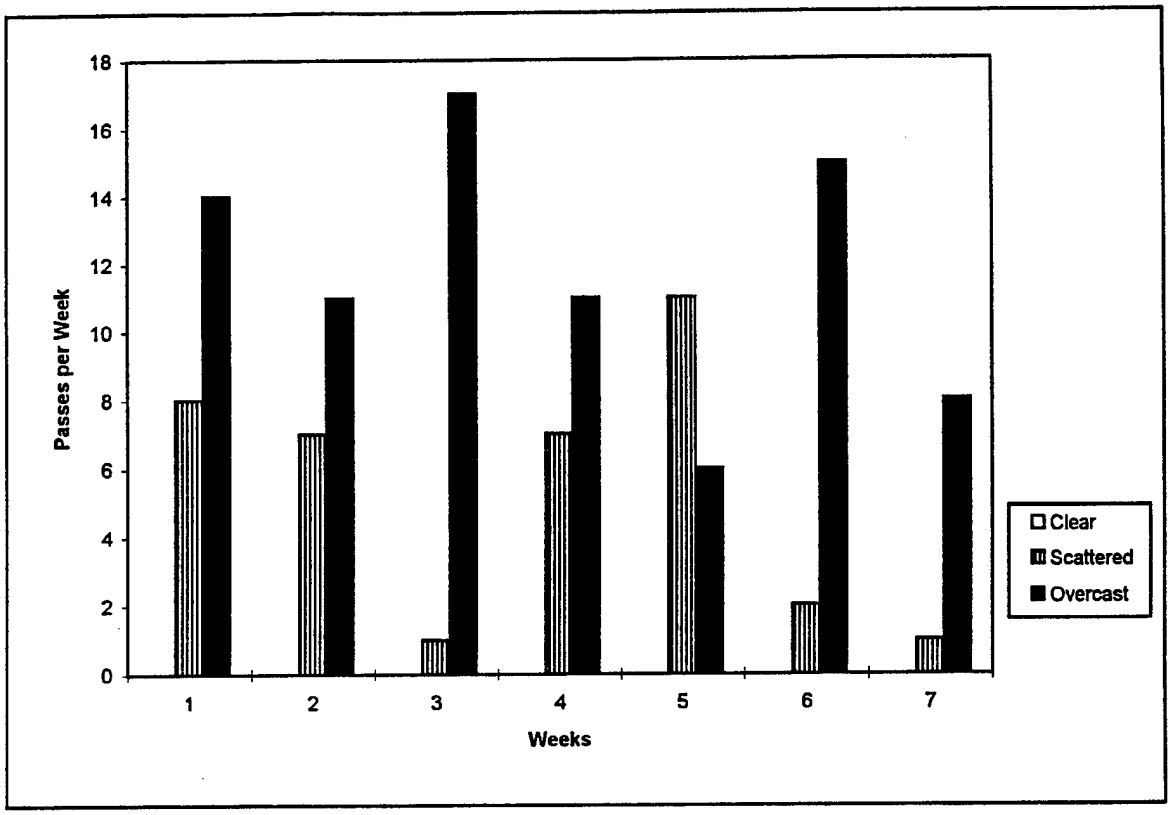


**Figure 5.** Total number of clear, scattered clouds, and cloudy images collected per week during Cape Race experiment.

Inspection of each image pair reveals that for most of the pairs the coincident cloud-free areas are too small for accurate velocity estimation. Of the 24 image pairs that satisfy the time constraint, only five image pairs, or about 21%, had large enough coincident cloud-free regions to allow velocity estimation. However, four of these image pairs could not be navigated accurately due to cloud cover over the ground control points making velocity estimation impossible. Only one image pair was suitable for velocity estimation. The image pair consists of the passes on day 317, hour 21, and day 318, hour 11, with a pass separation of 14 hours.

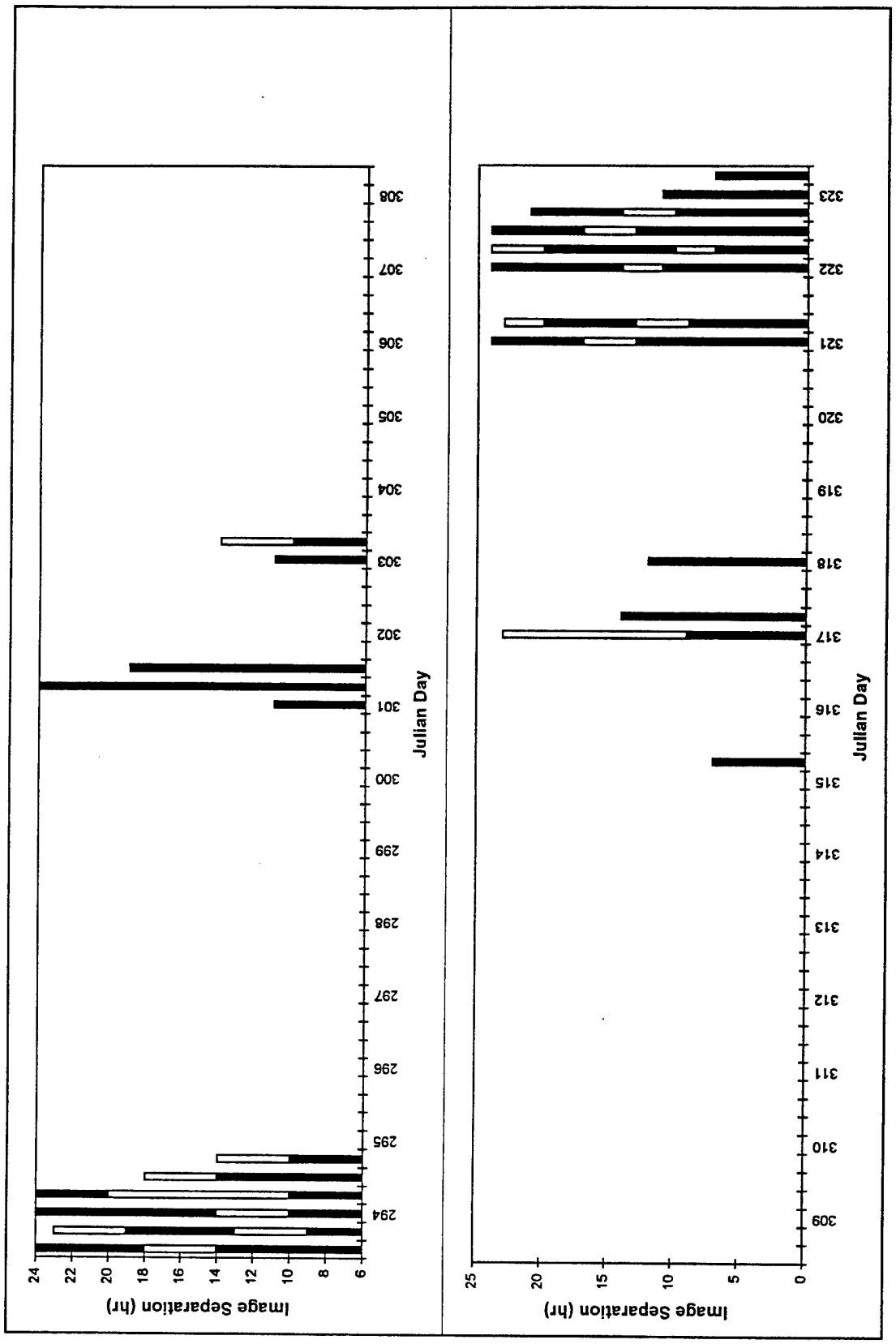


**Figure 6.** Cape Race experiment image pairs that satisfy the time constraint for velocity estimation by the heat inversion technique.

**Results**

The Cape Race Experiment resulted in disappointingly few usable images. After comparing the times and cloud cover of the images, only one image pair suitable for estimating surface velocities was obtained. The resulting velocity field is shown in Figure 7. The confidence level in these velocity estimates is low, particularly in the region of the Labrador Current. The estimated velocities appear to cross the Labrador Current perpendicularly. This is not physically realistic and is probably caused by the excessive cloud cover and the limited number of pixels that are cloud-free in both images. The estimates from this experiment are insufficiently accurate to be used for search planning.

## 5.2 1993 DELAWARE COASTAL CURRENT

From 22 March to 24 June 1993 (Julian days 81 - 175), ISARC supported the Delaware Coastal Current (DCC) Experiment performed by Dr. Richard Garvine of the Graduate College of Marine Studies, University of Delaware. The DCC can be subdivided into four subregions: 1) the source region near the estuary mouth, 2) the plume region, 3) the coastal jet region, and 4) the dissipation region (Figure 8). The outflow from the Delaware Bay occurs on the southern side of the bay's entrance. Typical speeds are 15 cm/s. Elsewhere the flow has a much weaker landward component. The horizontal plume shape initially spreads buoyant water offshore as it leaves the source region and then turns back toward the coast. The DCC responds differently to downwelling (southward) versus upwelling winds. During downwelling favoring winds the DCC flows at speeds of over 30 cm/s landward. During upwelling favoring winds, the DCC slows and spreads offshore. The plume region exhibits strong meandering. The meandering crests may detach to form eddies of buoyant water. Downstream of the plume region is a narrow, coastal jet region where the flow is more nearly longshore. At the downstream end, the current breaks into eddies of buoyant water (Münchow and Garvine, 1993).

The experiment used two independent methods to measure the sea surface current. About 40 drifters were deployed in the source region of the DCC during the experimental period. Drifters provide much better spatial coverage of the coastal current than arrays of moored instruments and yield results relevant to both Eulerian and Lagrangian frameworks.

The drifting buoy design is based on the Davis CODE drifter which consists of a slender, vertical, negatively buoyant tube with four, square drag-producing vanes extending most of the length of the tube. Buoyancy is provided by four small floats attached to the ends of the drag vanes (Davis, 1985). The drifters were drogued at 1 m depth.

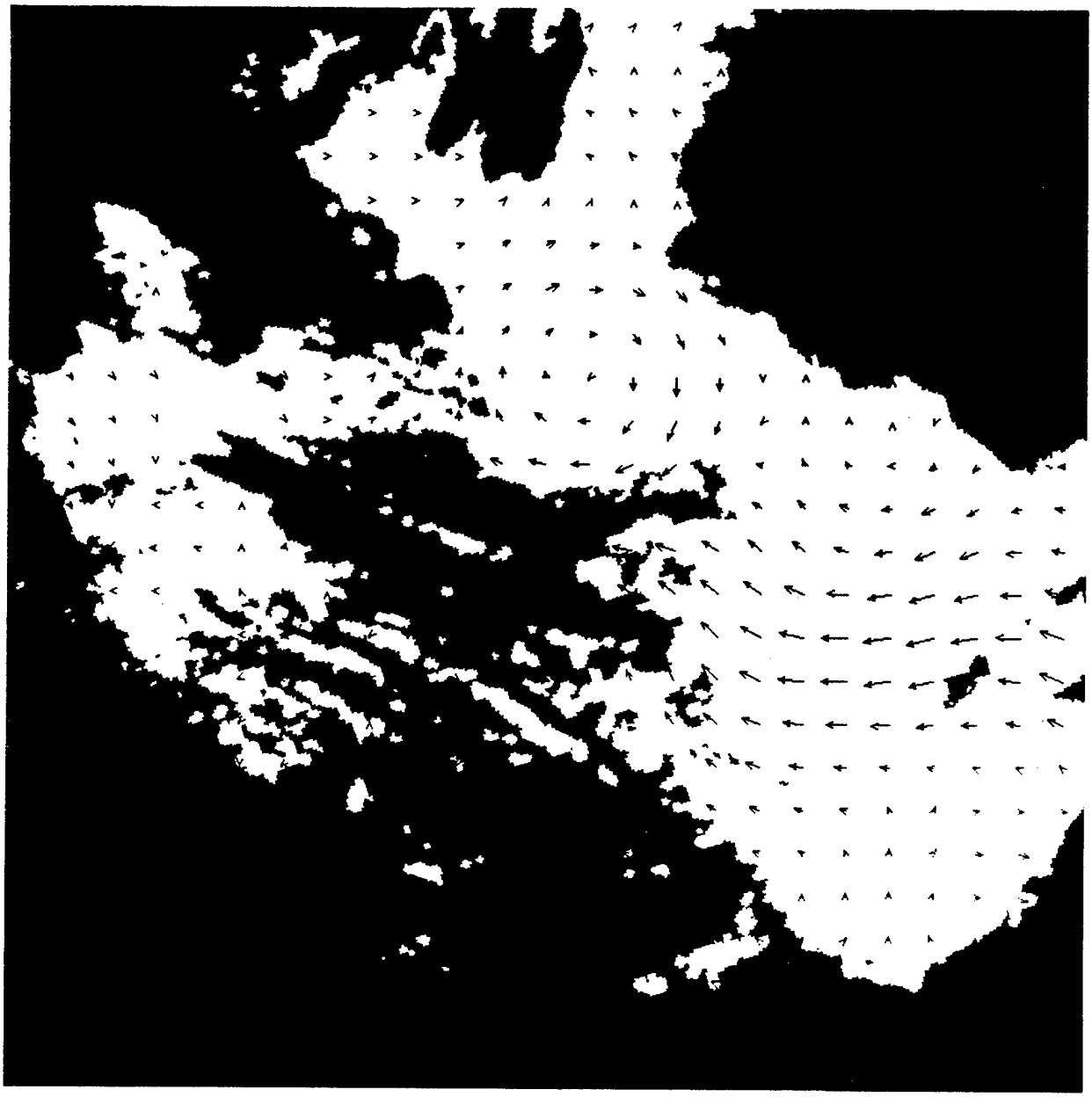

**Figure 7.** Velocity field off Cape Race, Newfoundland, on 12-13 November 1992.

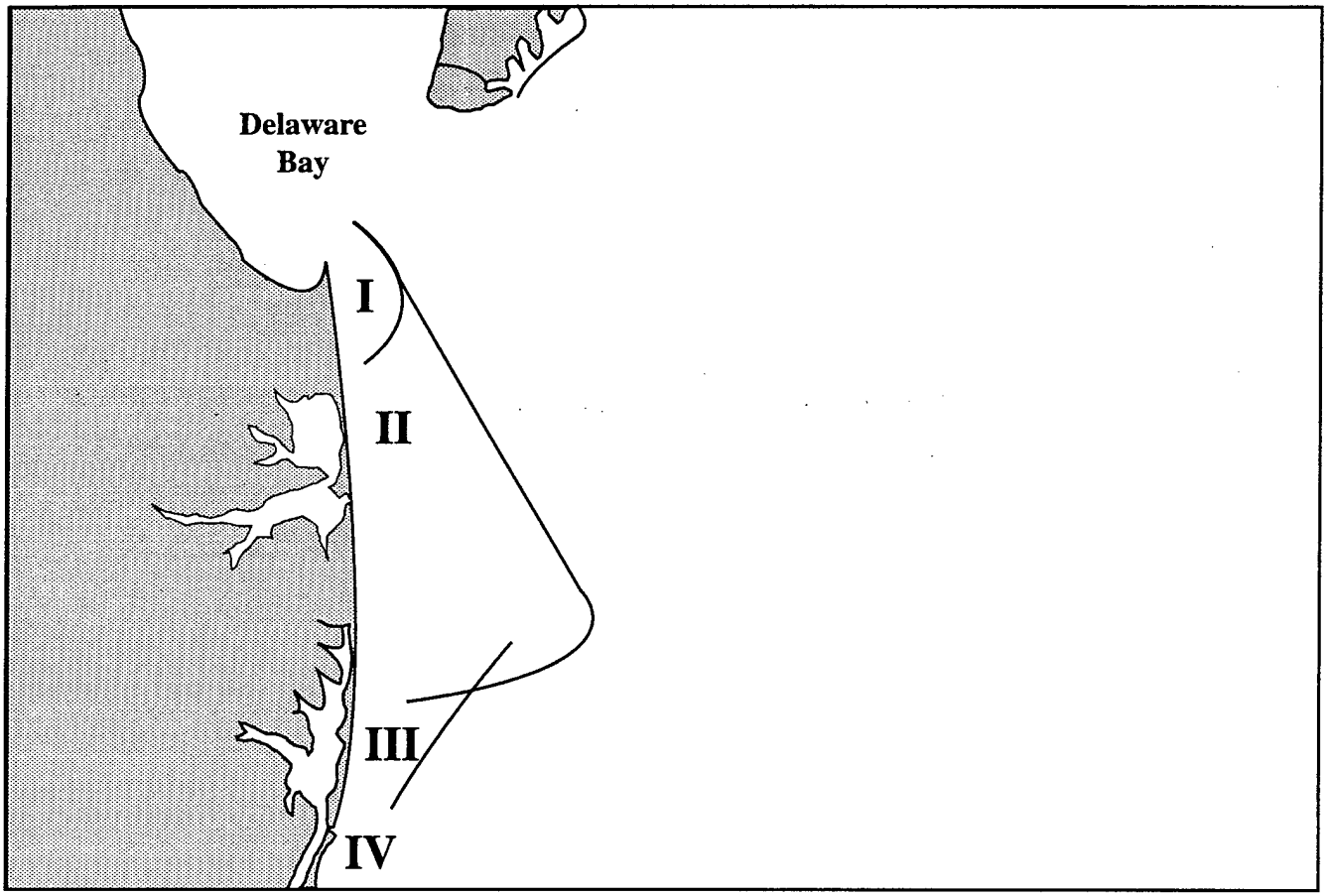


**Figure 8.** Subregions of the DCC: I) source region, II) plume region, III) coastal jet, and IV) dissipation region (Münchow and Garvine, 1993).

The second current measurement method was the underway recording of current data using a shipboard ADCP. An RDI, Inc. 1200 kHZ transducer set was towed abeam of the R/V Cape Henlopen in a shallow draft flotation housing. By using 1 m vertical resolution, usable returns were obtained for depths greater than 2 m depth which is sufficiently shallow for resolving most of the coastal current.

Current meter arrays provided current measurements at three locations across the source region of the DCC (Figure 8). All three current meter arrays had S4s at 2, 6, and 10 m depth. The middle array was moored in deeper water and had an additional S4 at 14 m depth.

Drifters were deployed along the source region sampling line four times over the three months of general sampling from March through June of 1993 when the river discharge normally is high and the DCC strongest (see Table 2 for dates). Between 11 and 14 drifters were deployed each time at uniform intervals of surface salinity, as determined from a portable conductivity-temperature-depth (CTD) sensor. In total, about 50 drifter trajectories were obtained during a variety of longshore wind and river discharge conditions.

**Table 2.** Dates of research cruises, buoy deployments, and recoveries during the 1993 DCC Experiment.

| | Dates | Julian Day | No. Buoys Deployed |
|---|---|---|---|
| Mapping Cruises | 3-5 April | 93-95 | — |
| | 29-30 April | 119-120 | — |
| | 1-3 May | 121-123 | — |
| | 5-6 June | 156-160 | — |
| Drifting Buoy Deployment/Recovery | 26 March<br>5 April | 85<br>95 | 14 |
| | 23 April<br>3 May | 113<br>123 | 11 |
| | 10 May<br>15 May | 130<br>135 | 13 |
| | 26 May<br>11 June | 147<br>162 | 13 |

Four separate shipboard and aircraft surveys of the coastal current fields were conducted at approximately monthly intervals, beginning in early April. Each shipboard survey consisted of two parts. The first part was a two-day survey of hydrographic conditions along a southward saw-tooth track. After a pause for one day to recover drifters, the hydrographic survey on the saw-tooth track was repeated northward.

## AVHRR Data

The AVHRR images were registered to a grid that extends from approximately 36°48'N to 39°34'N and from 73°42'W to 76°12'W. Figure 9 shows an image from 11 May 1993, 12 Z. Clouds are represented by dark grey and the land is masked to black. Figure 10 shows the total number of passes captured each week during the experiment. Of the 243 passes captured, 9% (23 images) were cloud-free, 34% (82 images) had scattered clouds and 57% (138 images) had clouds over the entire study region. Figure 11a shows the image pairs that satisfy the time constraint of a separation of 6 to 24 hours. As in Figure 6, these are identified as images separated in time between 6 and 24 hours. It can be seen that for a given image there may be more than one image pair that fits this time constraint. Inspection of each image pair reveals that for most of the pairs the coincident cloud-free areas are too small for accurate velocity estimation. Figure 11b shows the image pairs that meet the time constraint and have sufficient coincident cloud-free areas for velocity estimation. Of the 121 image pairs that satisfy the time constraint, 60 image pairs, or about 50%, had large enough coincident cloud-free regions to allow velocity estimation. Note in Figure 11b that these image pairs are not spaced evenly throughout the experimental period, but are restricted to times of fair weather. Several of these image pairs overlapped in time; selecting the best images (those nearest the 12 hour optimal separation) reduces the number of image pairs to 35. Table 3 lists the dates and times of the resulting image pairs.

## Results

To assess the accuracy and feasibility of using AVHRR velocity estimates from the inversion of the heat equation method for USCG search planning, comparisons were made between related AVHRR velocity solutions and between AVHRR estimates and drifting buoy data. Estimating surface velocities from AVHRR imagery will always involve subjective decisions by the operator, such as optimal image pair time separation and the value of the weighting parameter, $\alpha$, on the divergence. AVHRR velocity estimates were compared with the more direct methods of current measurement to assess the significance of these factors on the estimated velocity field.

**Figure 9.** SST from the AVHRR image on 11 May 1993, 12 Z.

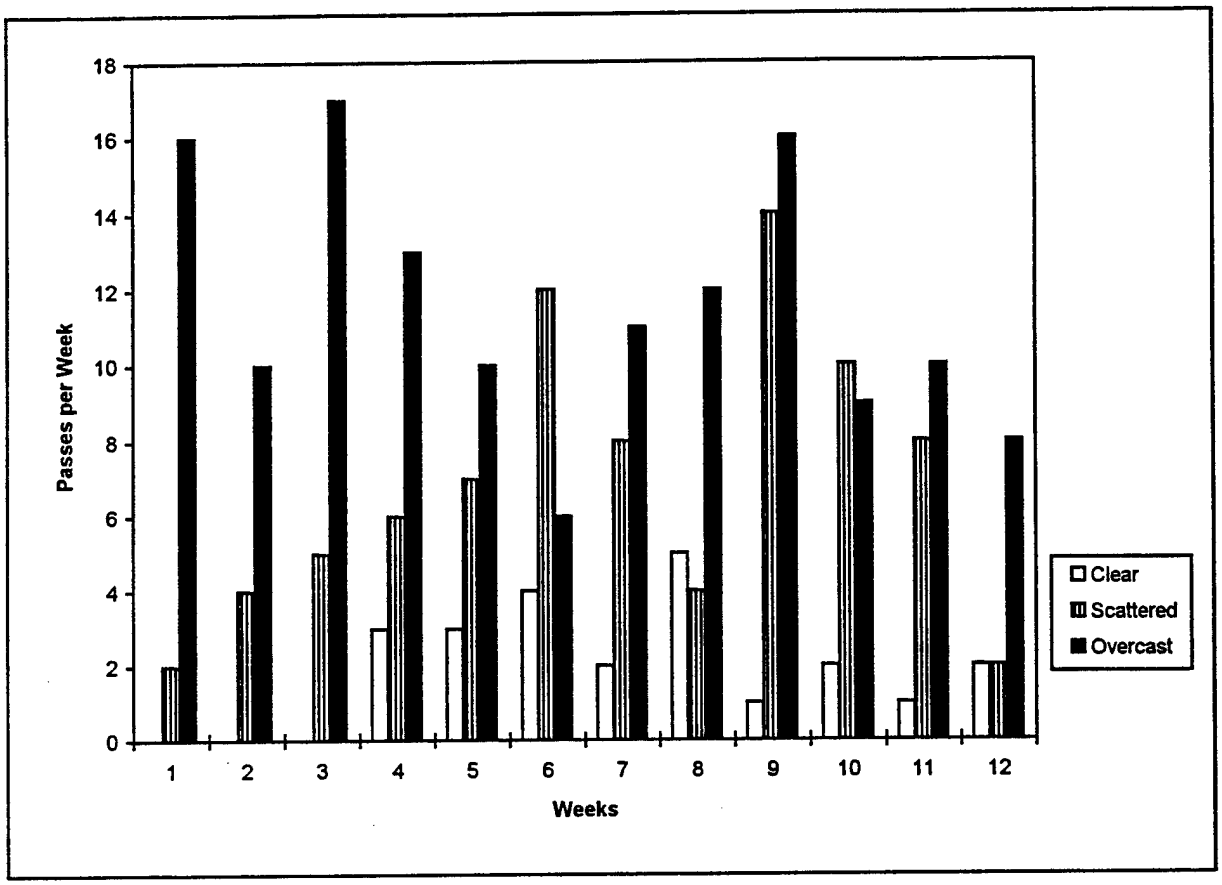


**Figure 10.** Total number of clear, scattered clouds, and cloudy images collected per week during the 1993 DCC Experiment.

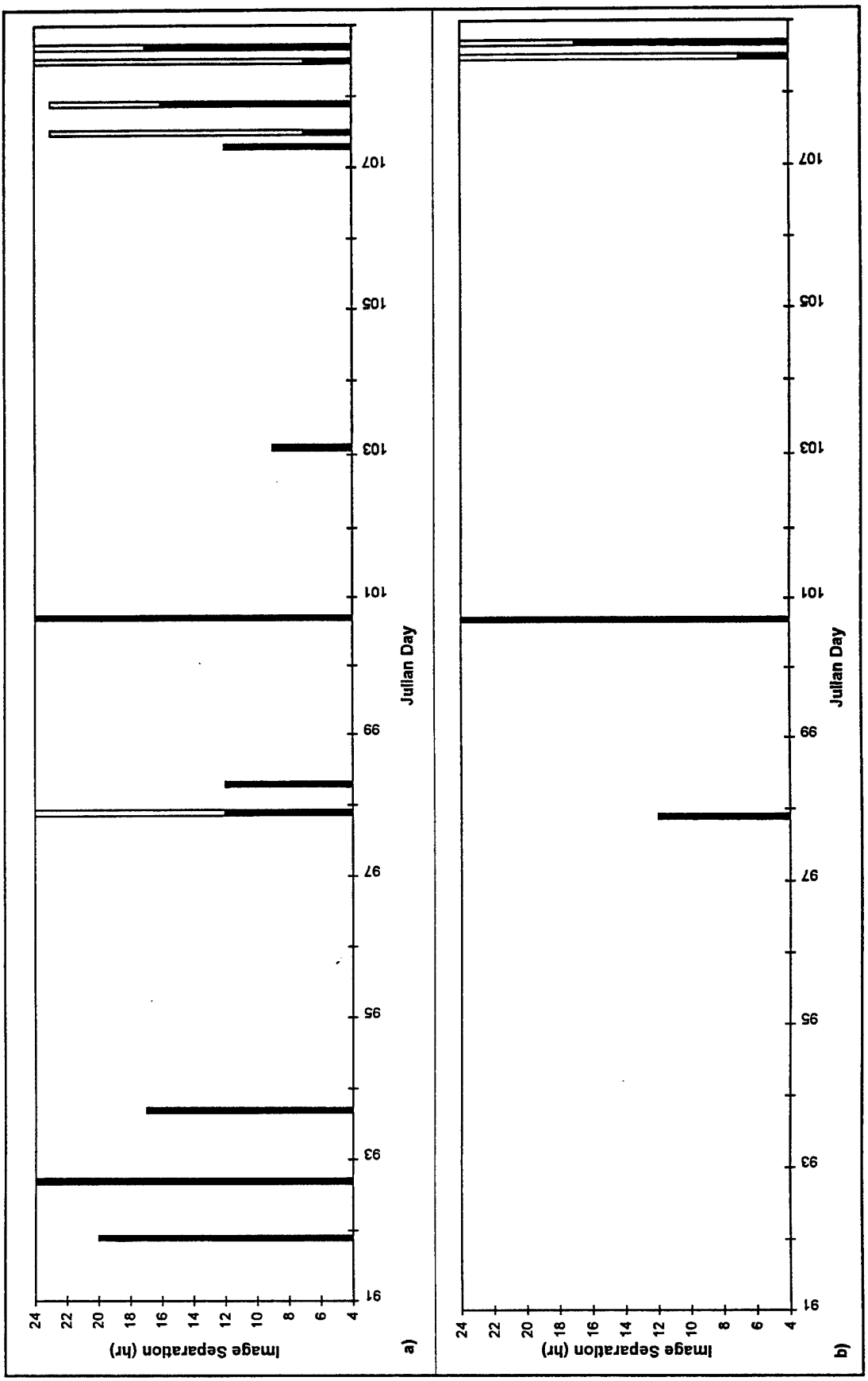


**Figure 11-1.** Image pairs that satisfy time and cloud conditions constraints during the 1993 DCC Experiment.

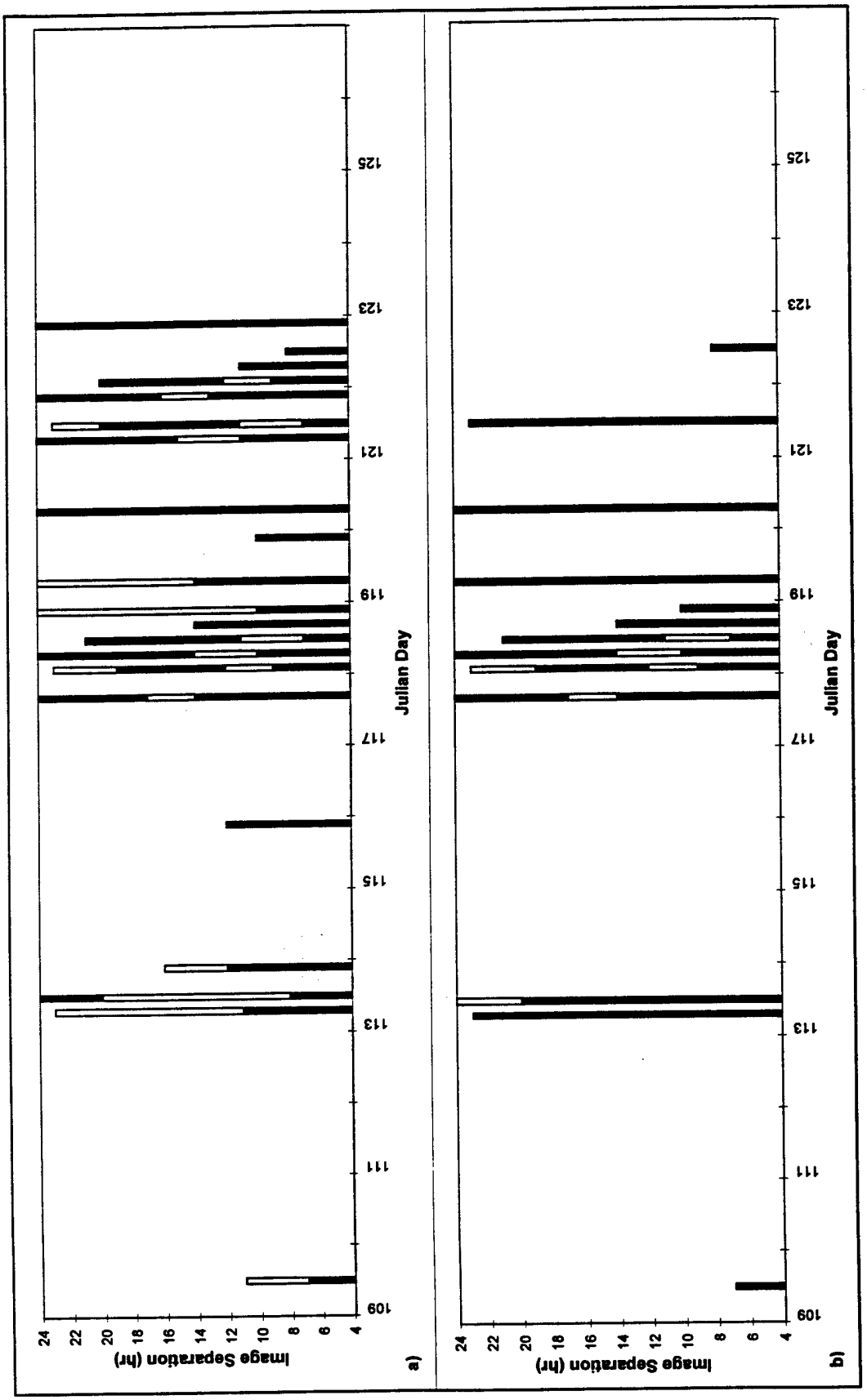


**Figure 11-2.** Image pairs that satisfy time and cloud conditions constraints during the 1993 DCC Experiment (Cont'd).

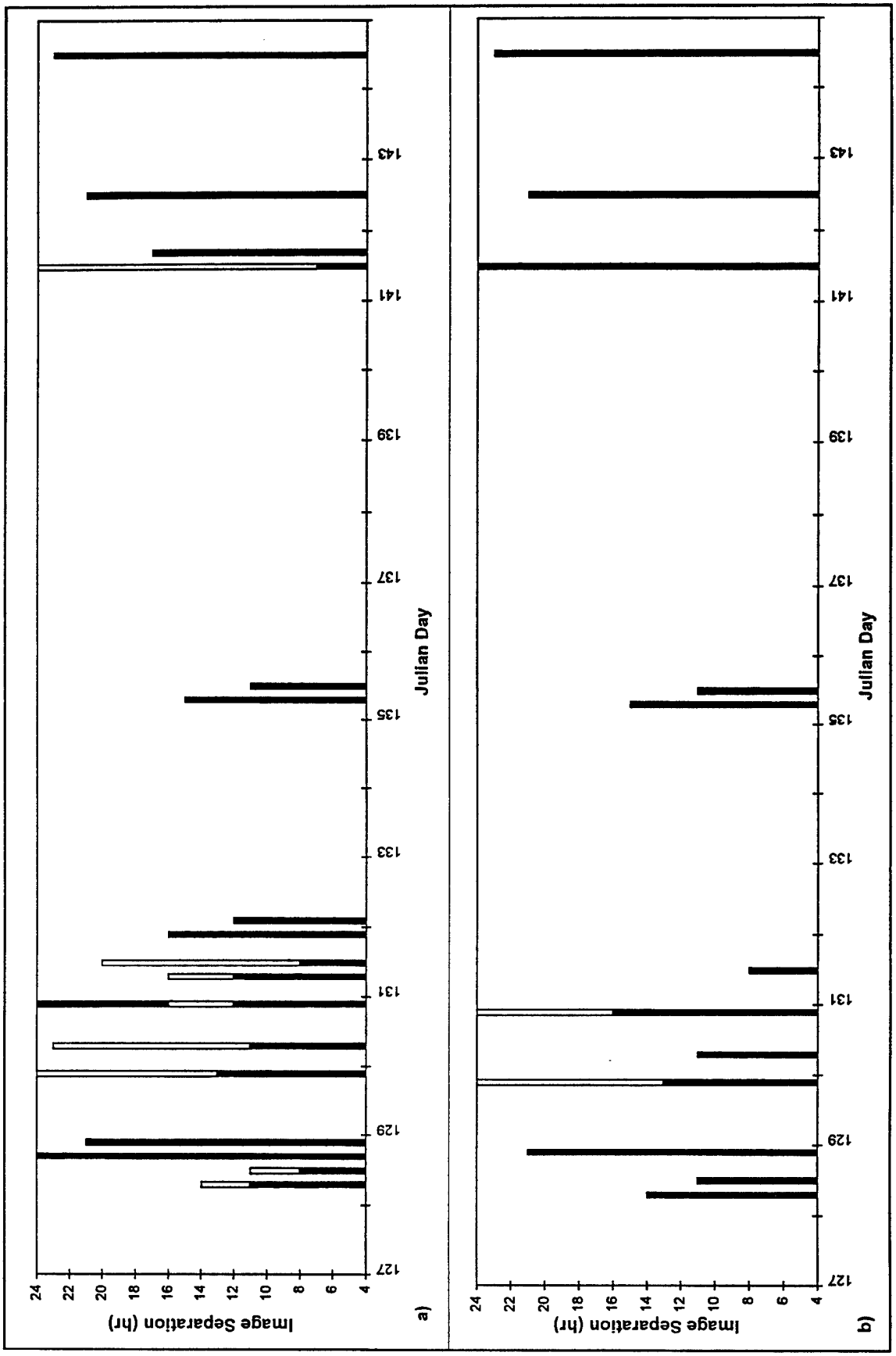


**Figure 11-3.** Image pairs that satisfy time and cloud conditions constraints during the 1993 DCC Experiment (Cont'd).

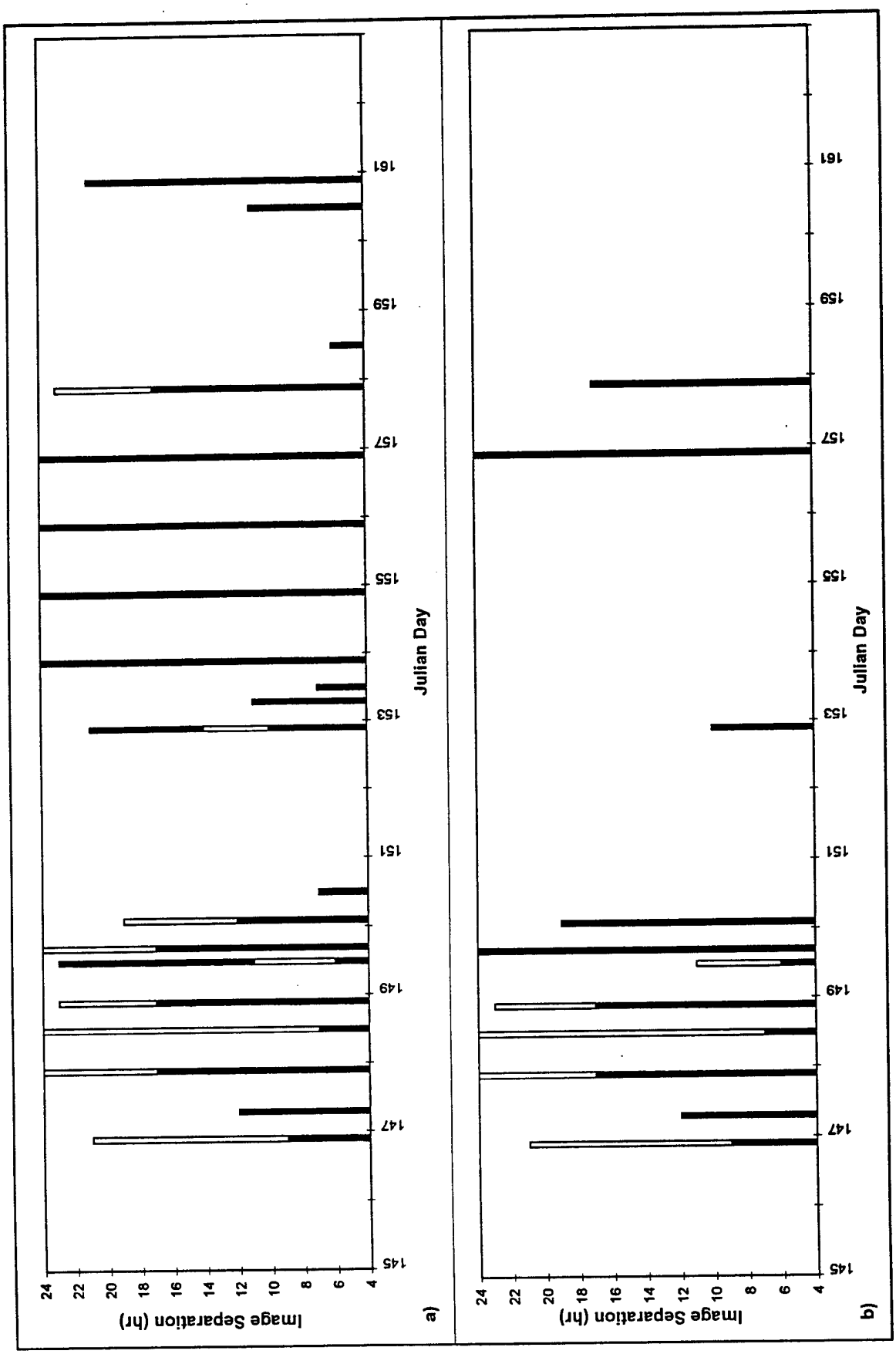


**Figure 11-4.** Image pairs that satisfy time and cloud conditions constraints during the 1993 DCC Experiment (Cont'd).

**Table 3.** Image pairs suitable for velocity estimation for the 1993 DCC Experiment.

| IMAGE PAIRS | | | | | |
|---|---|---|---|---|---|
| IMAGE 1 DAY:TIME | IMAGE 2 DAY:TIME | TIME SEP. (HOURS) | IMAGE 1 DAY:TIME | IMAGE 2 DAY:TIME | TIME SEP. (HOURS) |
| 97:20 | 98:8 | 12 | 130:9 | 130:20 | 11 |
| 100:19 | 101:19 | 24 | 130:20 | 131:12 | 16 |
| 108:12 | 108:19 | 7 | 131:12 | 131:20 | 8 |
| 108:19 | 109:12 | 17 | 135:13 | 136:00 | 11 |
| 109:12 | 109:19 | 7 | 141:12 | 142:12 | 24 |
| 113:12 | 114:8 | 20 | 142:12 | 143:9 | 21 |
| 113:12 | 114:12 | 24 | 144:13 | 145:12 | 23 |
| 117:19 | 118:9 | 14 | 146:23 | 147:8 | 9 |
| 118:00 | 118:12 | 12 | 147:8 | 147:20 | 12 |
| 118:9 | 118:19 | 10 | 147:20 | 148:13 | 17 |
| 118:19 | 119:9 | 14 | 148:13 | 148:20 | 7 |
| 119:9 | 120:9 | 24 | 148:20 | 149:13 | 17 |
| 120:9 | 121:9 | 24 | 149:13 | 150:00 | 11 |
| 121:13 | 122:12 | 23 | 150:00 | 150:19 | 19 |
| 122:12 | 122:20 | 8 | 152:23 | 153:9 | 10 |
| 128:12 | 128:23 | 11 | 156:20 | 157:20 | 24 |
| 128:23 | 129:20 | 21 | 157:20 | 158:13 | 17 |
| 129:20 | 130:3 | 13 | — | — | — |

***Effect of weighting parameter on AVHRR velocity estimate*** - By varying the weighting parameter, $\alpha$, on the divergence, the inversion of the heat equation produces a family of solutions (Kelly and Strub, 1992). It is envisioned that it will not be operationally feasible to generate a family of solutions and then determine the optimum value of $\alpha$. Therefore, the velocity fields for a range of weighting parameters, $\alpha$, were calculated and the estimates compared. An image pair from April 28 (Julian day 118, 12 and 23 Z) was selected to assess the influence of $\alpha$ on the estimated velocity field. Six solutions were computed for the image pair with $\alpha$ varying from 0.01 to 0.5 (see Figure 12). The maximum estimated velocity for the image pair varied between 17 and 31 cm/s. For each of the weighting parameters examined, the maximum estimated velocity was on the eastern edge of the eddy located in the lower center of the image (see Figure 12). The current direction at this location varied, depending on the weighting parameter selected, between 96.2° and 106.2°. The RMS velocity over the image varied between 5 and 11 cm/s. For this image pair the maximum difference in the estimated velocity at a point as a result of varying the value of $\alpha$ from 0.01 to 0.5 was 34 cm/s. The minimum difference was as low as 5 cm/s. The minimum value occurred in the eddy in the lower center of the image. The mean difference in velocity estimates over the image ranged between 1 and 5 cm/s. The trigonometric mean difference in direction ranged between 3 and 17°. Comparison of Figures 12a and 12f reveals the effect of $\alpha$ on smoothing the velocity field. The velocity field shown in Figure 12a ($\alpha$=0.01) is less coherent than that shown in Figure 12f ($\alpha$=0.5). The velocity field changes gradually with increasing $\alpha$. The value of $\alpha$ is selected subjectively to produce the most realistic total velocity field and velocity magnitudes and directions. The optimum value of $\alpha$ will vary from image pair to image pair depending on the influence of the divergence on the velocity field. The selection of the optimum value will depend on operator experience and interpretation.

***Comparison of AVHRR velocity estimates for two time separations*** - Image pairs with an optimal time separation of 12 hours will frequently be unavailable. The effect of using a shorter time separation was examined by comparing the current estimated from images separated by 7 and 11 hours (Julian day 118, 12 and 19 Z, and 12 and 23 Z). A time separation of 7 hours between the images resulted in higher maximum velocity estimates and higher mean velocity estimates over the imaged region for each value of $\alpha$ examined. The maximum velocity was greater by 29 to 52% (10-30 cm/s) depending on the value of $\alpha$. However, the pixel with the maximum estimated velocity was not always in the same location for the two time separations. Comparing the velocity for the 7-hour separation at the same location as the maximum velocity for the 11-hour separation, the velocity for the 7-hour separation was lower by 7 to 21% depending on the value of $\alpha$. The mean estimated velocity over the image was greater for the 7-hour separation by approximately 25 to 47% (0.2-3.7 cm/s).

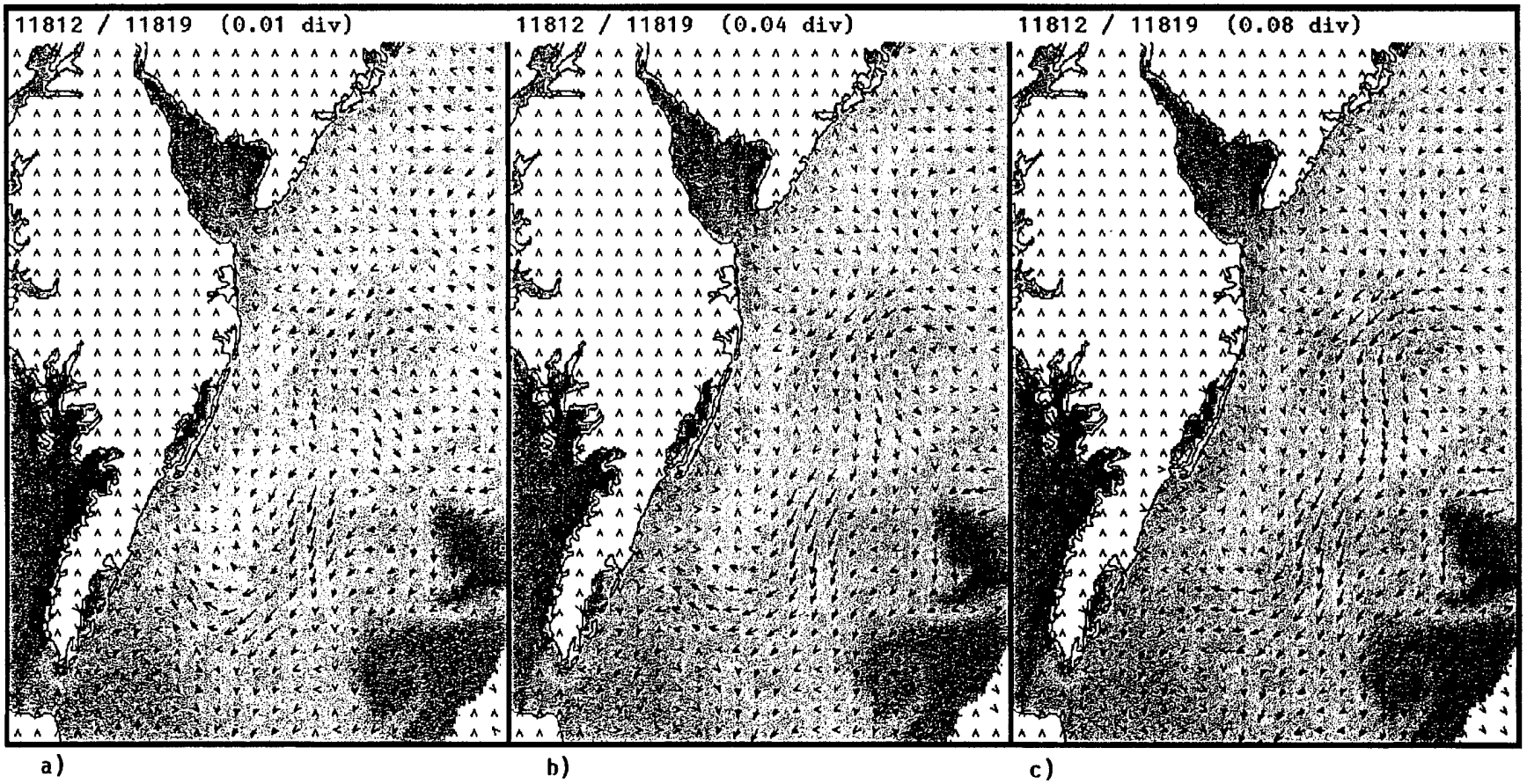


**Figure 12-1.** Family of velocity solutions derived from the inversion technique for April 23, 12 and 23 Z.

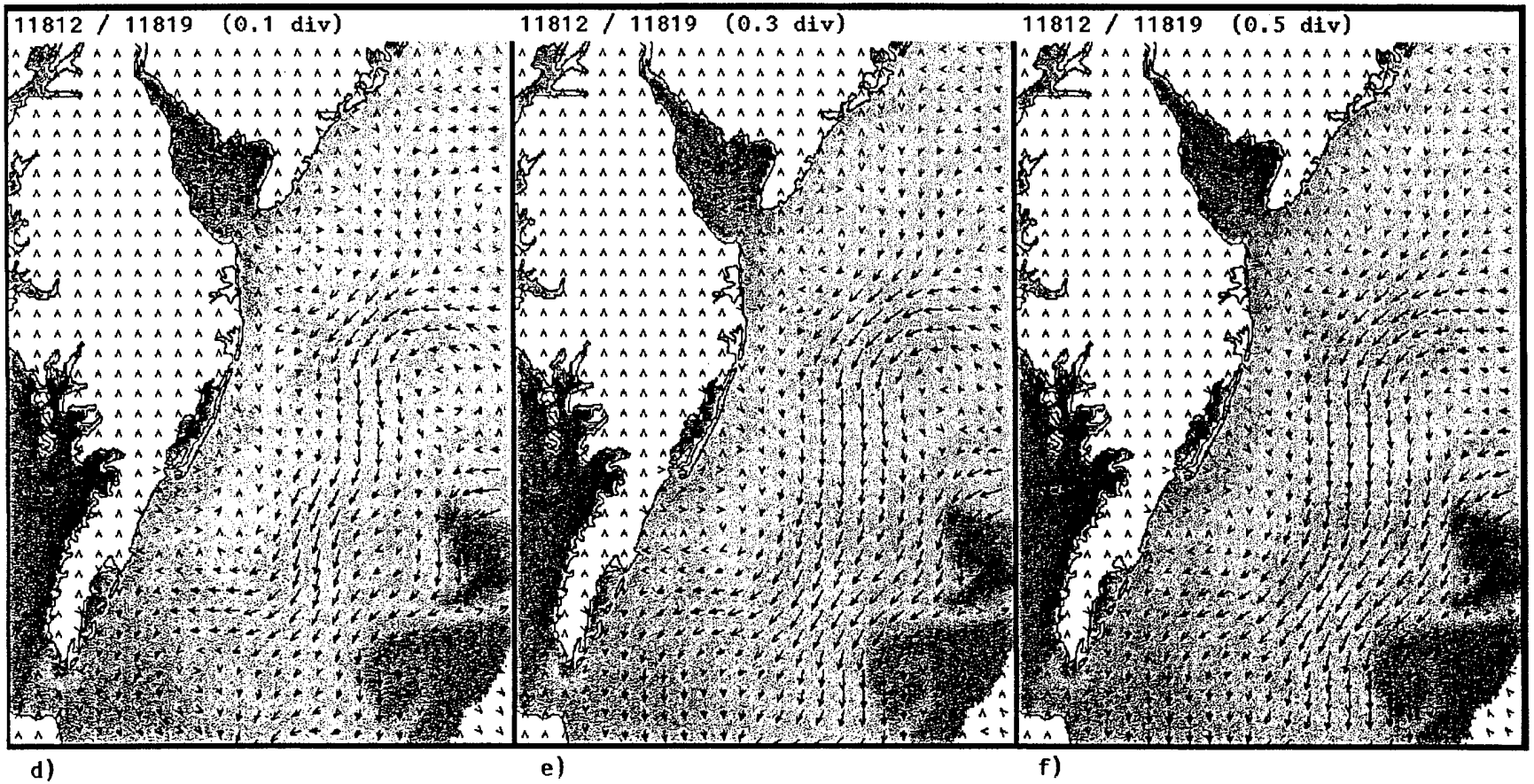


**Figure 12-1.** Family of velocity solutions derived from the inversion technique for April 23, 12 and 23 Z (Cont'd).

***Comparison of AVHRR velocity estimates with drifter data*** - Although measurement of surface velocity using drifters is a more direct velocity measurement than AVHRR, it cannot be considered the "actual" velocity because it has its own sources of error (O'Donnell et al., 1995). However, discrepancies between the AVHRR estimates and the drifter measurements may suggest the magnitude of the errors in the AVHRR estimates. Drifter data from the second deployment were compared with the velocity estimates from April 28, 29 and 30 (Julian days 118 - 120). The images selected are listed in Table 4. To avoid errors inherent in the Argos positioning, only high quality drifter fixes separated by more than 23 hours were selected for comparison. Because the drifter measurements were spatially sparse compared with the AVHRR estimates, the drifter measurements from 12 hours before the initial image to 12 hours after the second image were combined for the comparisons. Between 7 and 10 drifter comparison vectors were used for each image pair. Figure 13 shows the AVHRR-derived current field overlaid with the drifter trajectories. A plot of the AVHRR-derived versus the drifter velocities is shown in Figure 14. When compared to the drifter velocities, the satellite-derived flow estimates had an overall RMS error of 23 cm/s and a trigonometric mean error in direction of about 19°. Comparing the interpolated AVHRR velocity estimates with the original drifter vectors gave a magnitude ratio (AVHRR/drifter) of 0.16. RMS velocity differences for each image pair/drifter comparison ranged between approximately 22 and 25 cm/s. Directional differences were between approximately 8° and 44° (see Table 5). Kelly and Strub (1992) found magnitude ratios (AVHRR/drifter) of approximately 0.3, which is considerably better than that determined from the 1993 DCC data. However, the directional differences in Kelly and Strub (1992) were much larger, ranging from 39° to 73°. These values represent the accuracy of the heat inversion technique. However, the absolute accuracy is affected by image quality, feature stability, time interval between images, and experience of the analyst (Svejkovsky, 1988).

**Table 4.** AVHRR image pairs used in the 1993 DCC Experiment velocity estimates.

| Day: Hour | Day/Night | Satellite | Day: Hour | Day/Night | Satellite | Time Sep. (Hours) |
|---|---|---|---|---|---|---|
| 118:12 | Day | NOAA 12 | 118:23 | Night | NOAA 12 | 11 |
| 118:19 | Day | NOAA 11 | 119:09 | Night | NOAA 11 | 14 |
| 118:23 | Night | NOAA 12 | 119:12 | Day | NOAA 12 | 13 |
| 119:09 | Night | NOAA 11 | 120:09 | Night | NOAA 11 | 24 |
| 120:09 | Night | NOAA 11 | 121:09 | Night | NOAA 11 | 24 |

**Table 5.** Comparison of drifter and AVHRR-derived surface currents for the 1993 DCC Experiment.

| Day:Hour | Ratio AVHRR/ Drifter | RMS Vel. Diff. (cm/s) | Directional Diff. | No. Drifters |
|---|---|---|---|---|
| 118:12 | 0.14 | 23.8 | 44.2° | 10 |
| 118:19 | 0.21 | 23.2 | 15.6° | 10 |
| 118.23 | 0.08 | 24.9 | 11.4° | 7 |
| 119:9 | 0.17 | 23.3 | 13.6° | 10 |
| 120:9 | 0.18 | 22.0 | 8.4° | 10 |

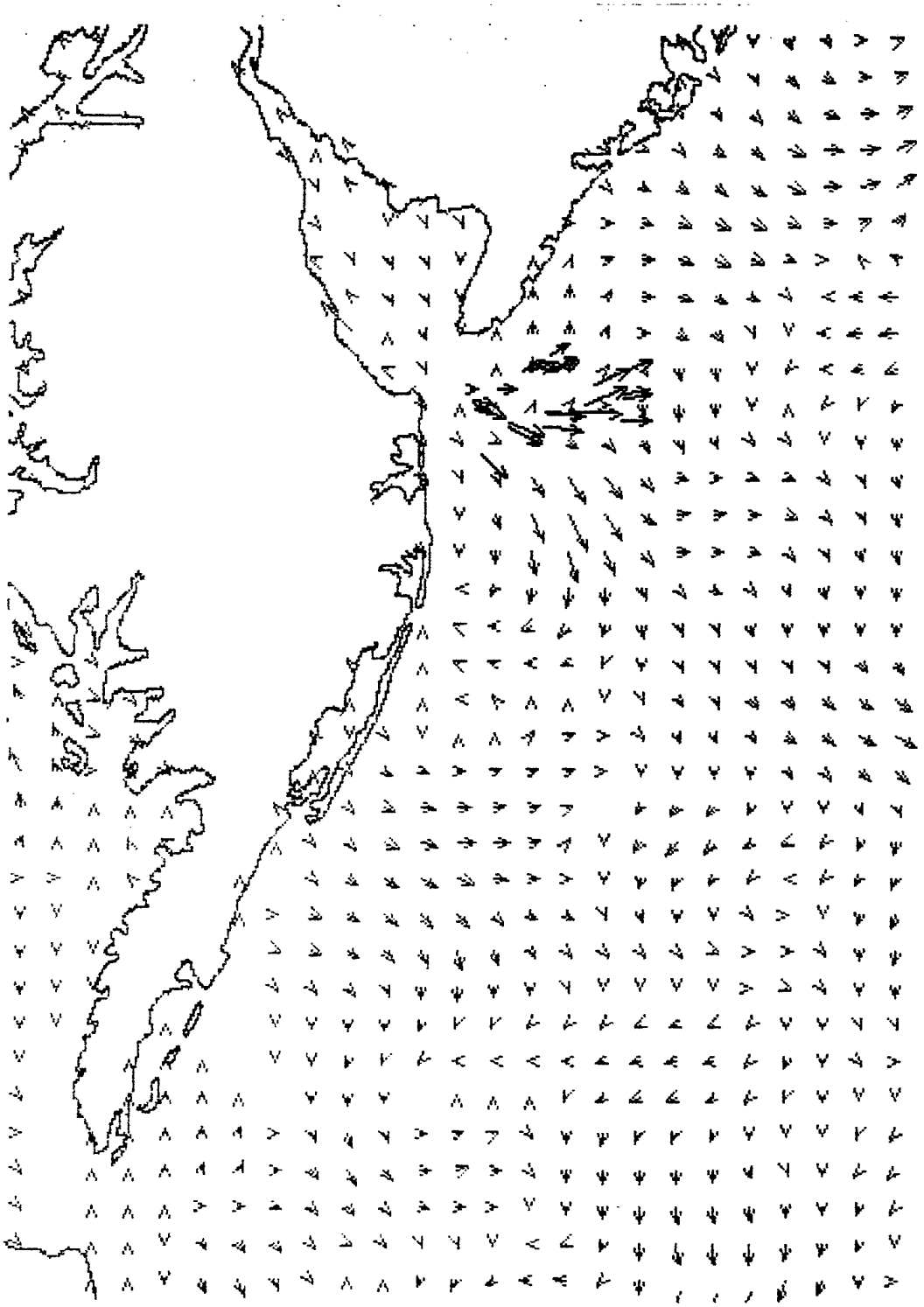

**Figure 13.** AVHRR-derived velocity estimates for image pair from 16 May 1993, 12 and 23 Z, overlaid with drifter velocities.

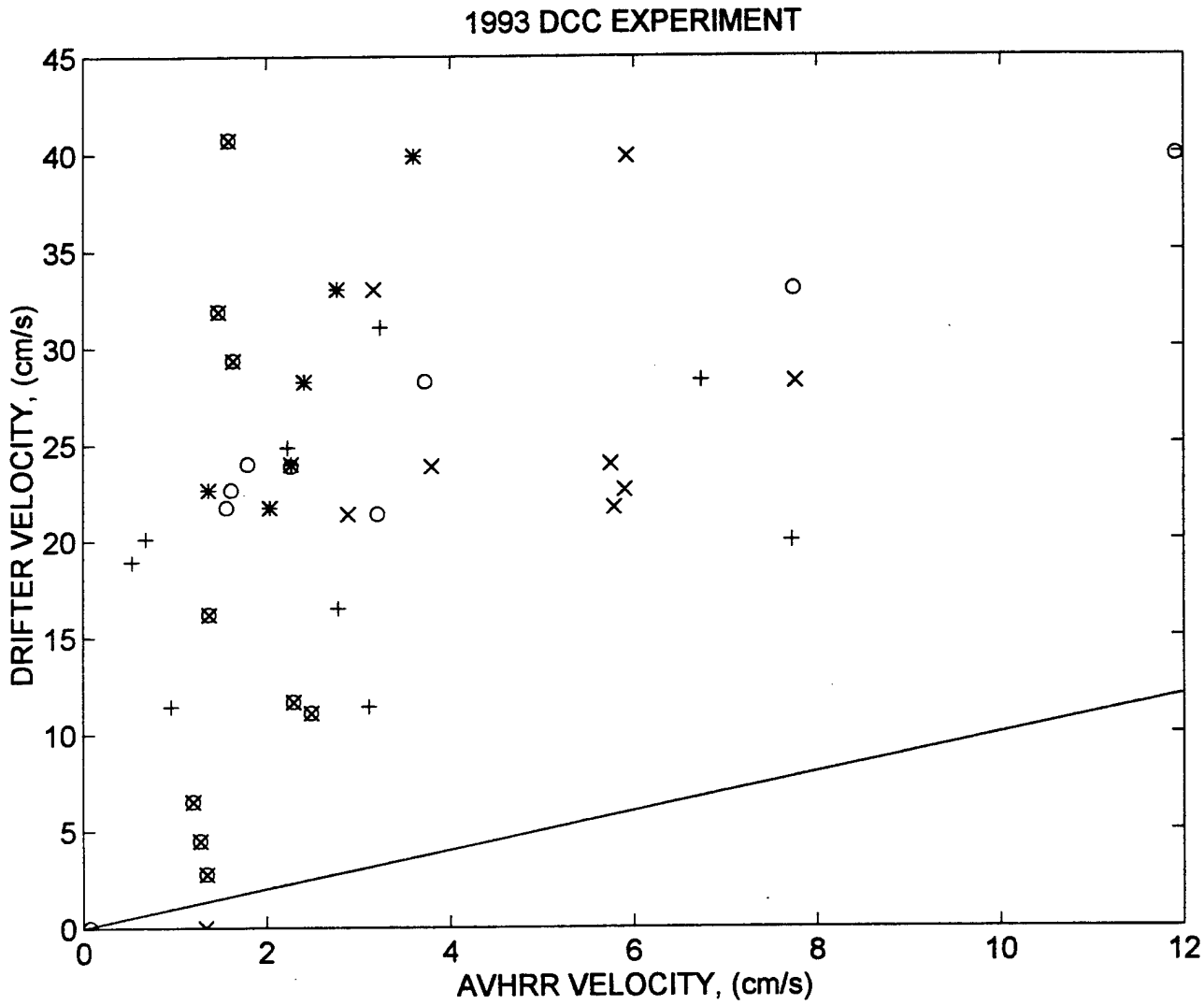


Figure 14. Drifter versus AVHRR-derived sea surface velocities for the 1993 DCC Experiment: (o) 28 April, 12 Z; (x) 28 April, 19 Z; (*) 28 April, 23 Z; (+) 29 April, 9 Z; (⊗) 30 April, 9 Z.

## 5.3 1994 DELAWARE COASTAL CURRENT

From 22 March to 16 May 1994 (Julian days 81 - 136), ISARC supported the 1994 DCC Experiment performed by Dr. Garvine. This experiment was similar in scope and method to the 1993 DCC Experiment. About 50 drifters were deployed in the source region of the DCC over the experimental period. The drifters were drogued at 3 m rather than at 1 m, as they were during the 1993 DCC Experiment. The drag producing vanes were removed to reduce the influence of windage on the drifter response. Drifters were deployed along the source region sampling line during March and April (see Table 6 for dates). Between 16 and 18 drifters were deployed each time. In total, about 50 (3 sets of 16-18) trajectories were obtained during a variety of longshelf wind and river discharge conditions. Three separate shipboard and aircraft surveys of the coastal current fields at approximately three weekly intervals were conducted, beginning at the end of March. The shipboard survey consisted of two parts, as during the 1993 DCC Experiment.

**Table 6**. Dates of research cruises, buoy deployments and recoveries during the 1994 DCC Experiment.

| | Dates | Julian Day | No. Buoys Deployed |
|---|---|---|---|
| Mapping Cruises | 29-30 March | 88-89 | — |
| | 18-19 April | 108-109 | — |
| | 2-4 May | 122-124 | — |
| Drifting Buoy Deployment/Recovery | 23 March<br>30 March | 82<br>89 | 18 |
| | 11 April<br>19 April | 101<br>109 | 16 |
| | 25 April<br>3 May | 115<br>123 | 16 |

## AVHRR Data

The AVHRR images were registered to the same grid as for the 1993 DCC Experiment. Figure 15 shows the total number of passes captured each week during the experiment. Of the 135 passes captured, 33% (45 images) were cloud-free, 25% (34 images) had scattered clouds and 42% (56 images) had clouds over the entire study region. Figure 16a shows the image pairs that satisfy the time constraint of a time separation between 6 and 24 hours. As shown previously, there may be more than one image pair that fits this time constraint. Inspection of each image pair reveals that for most pairs the coincident cloud-free areas are too small for accurate velocity estimation. Figure 16b shows the image pairs suitable for velocity estimation after comparison of cloud extent and location. Of the 130 image pairs that satisfy the time constraint, only 57 image pairs, or 44%, had large enough coincident cloud-free regions to allow velocity estimation. The impact of weather conditions on image availability was more evident during the 1994 DCC than in 1993. Figure 16b shows days with suitable image pairs are separated by several days without any pairs. Several of these image pairs overlapped in time; selecting the best images (those nearest the 12 hour optimal separation) reduces the number of image pairs to 34. Table 7 lists the dates and times of the resulting image pairs.

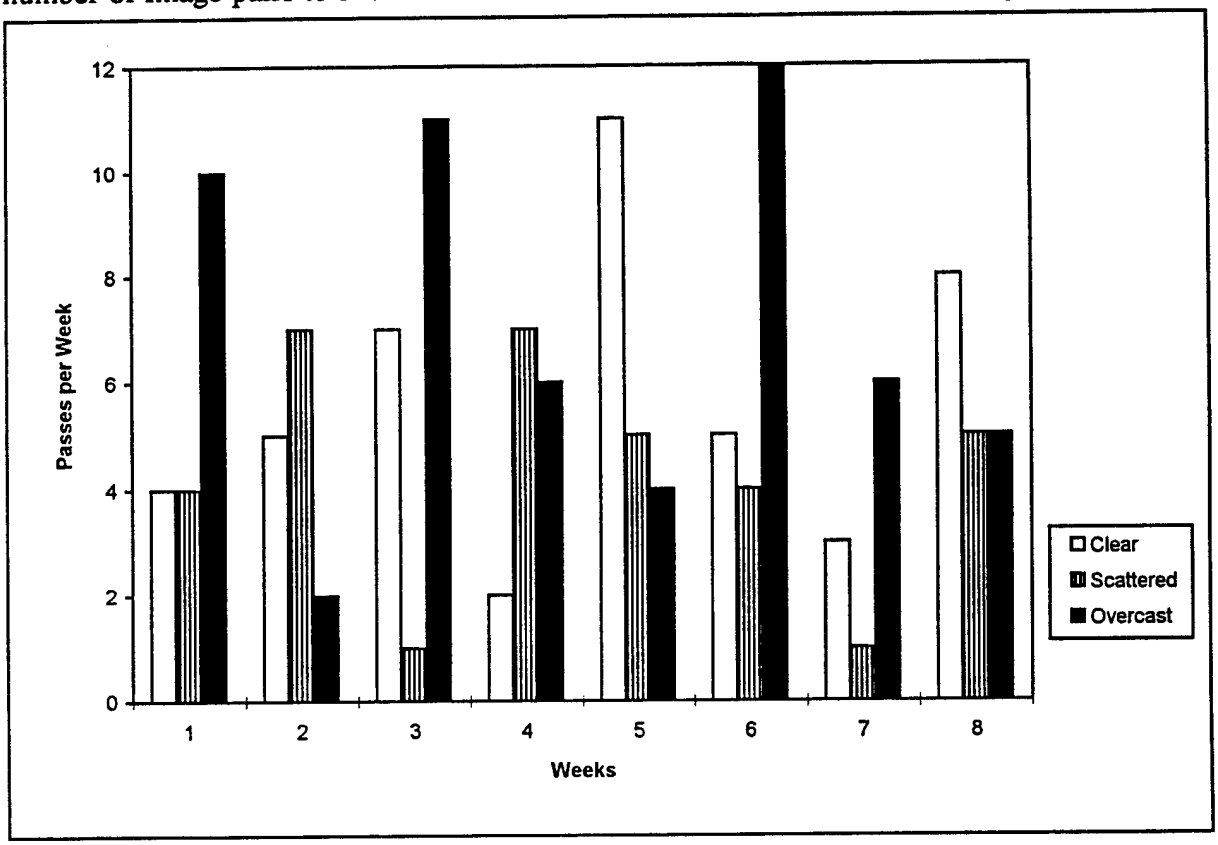


**Figure 15.** Total number of clear, scattered clouds, and cloudy images collected per week during 1994 DCC Experiment.

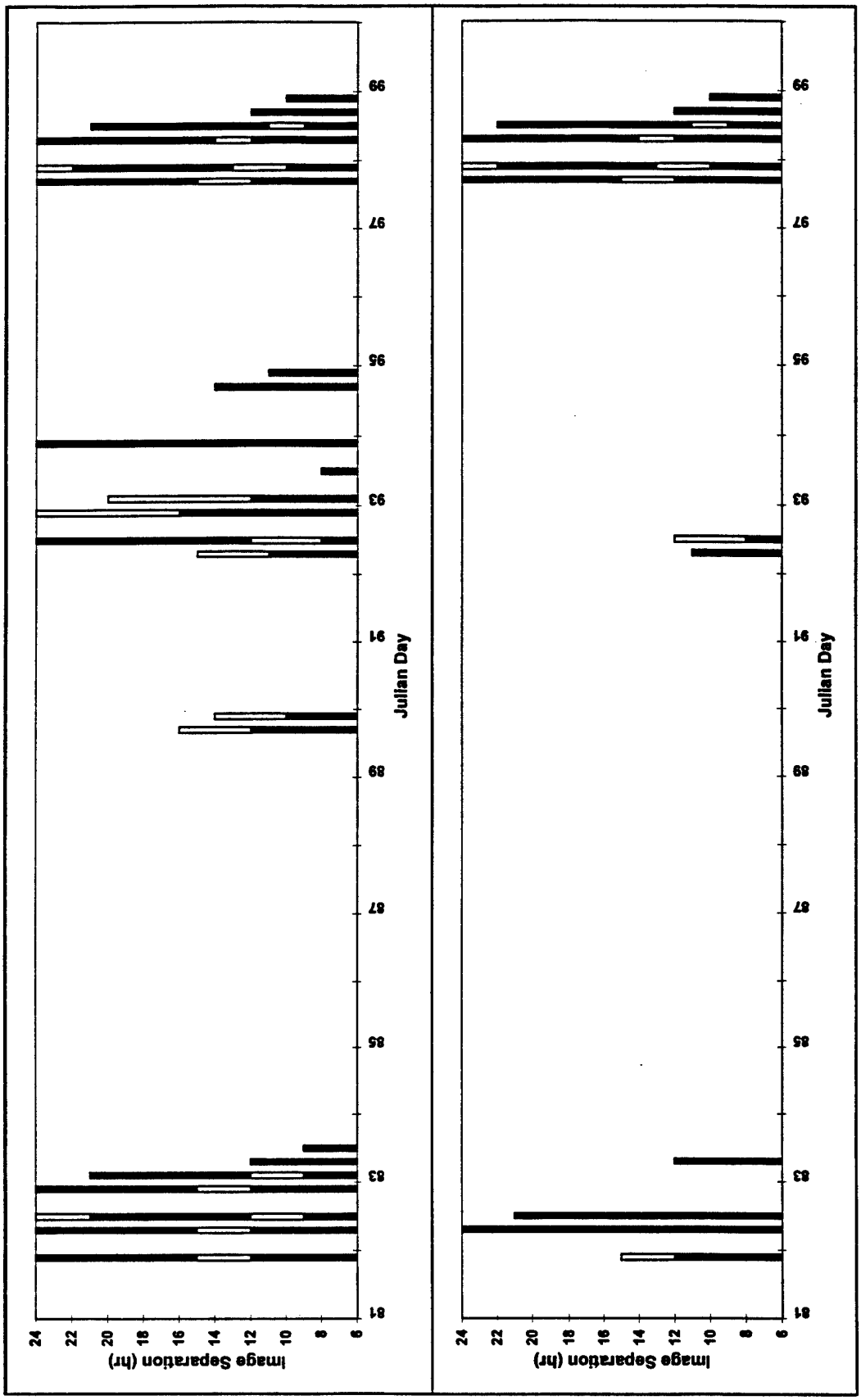


**Figure 16-1.** Image pairs that satisfy the time and cloud conditions constraints during the 1994 DCC Experiment.

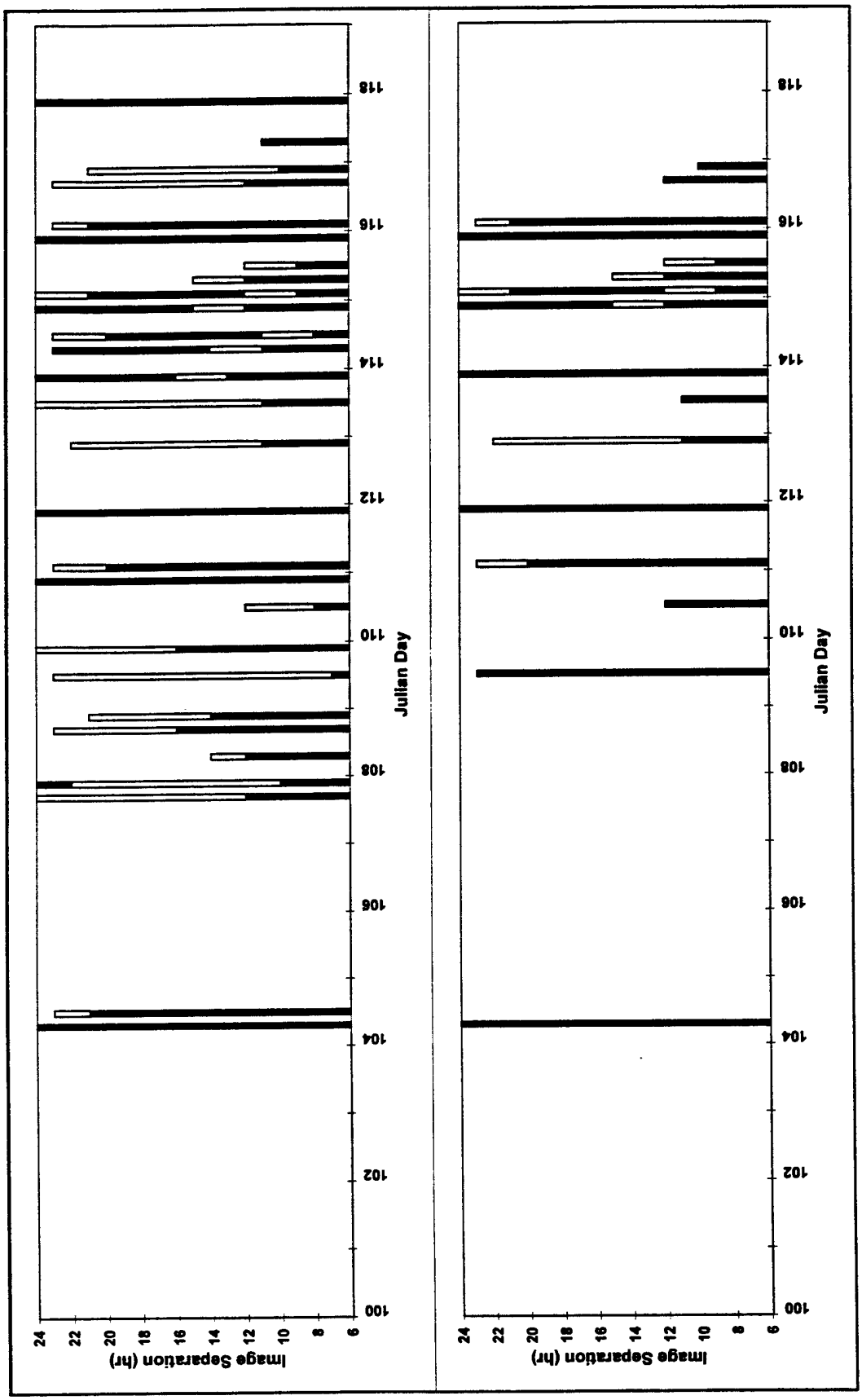


**Figure 16-2.** Image pairs that satisfy the time and cloud conditions constraints during the 1994 DCC Experiment (Cont'd).

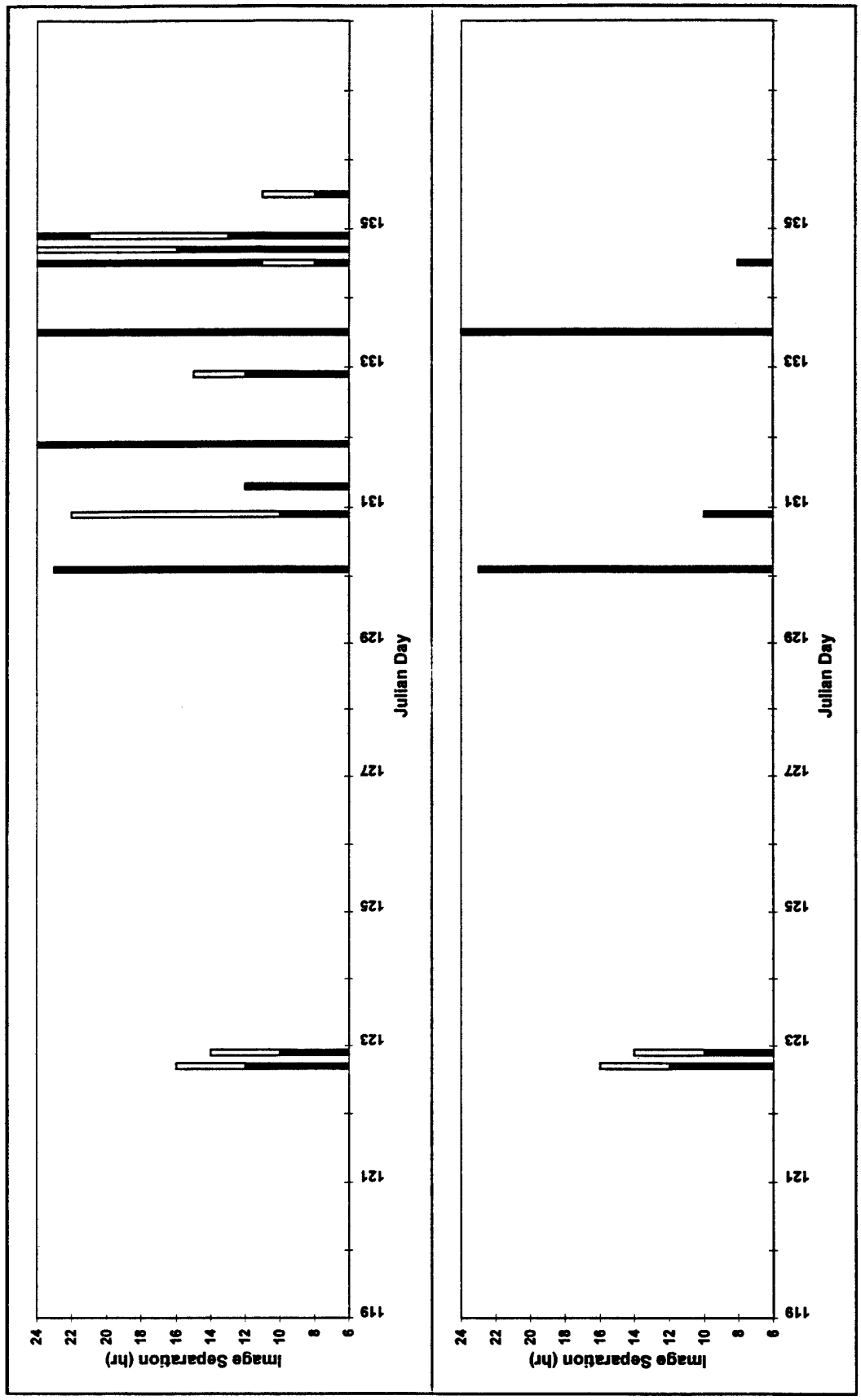


**Figure 16-3.** Image pairs that satisfy the time and cloud conditions constraints during the 1994 DCC Experiment (Cont'd).

**Table 7.** Image pairs suitable for velocity estimation for the 1994 DCC Experiment.

| IMAGE PAIRS | | | | | |
|---|---|---|---|---|---|
| IMAGE 1 DAY:TIME | IMAGE 2 DAY:TIME | SEPARATION, HOURS | IMAGE 1 DAY:TIME | IMAGE 2 DAY:TIME | SEPARATION, HOURS |
| 81:21 | 82:9 | 12 | 112:23 | 113:10 | 11 |
| 82:9 | 83:9 | 24 | 113:10 | 113:21 | 11 |
| 82:12 | 83:9 | 21 | 113:21 | 114:21 | 24 |
| 83:9 | 83:21 | 12 | 114:21 | 115:9 | 12 |
| 92:9 | 92:20 | 11 | 115:0 | 115:12 | 12 |
| 92:12 | 93:0 | 12 | 115:9 | 115:21 | 12 |
| 97:21 | 98:9 | 12 | 115:12 | 116:0 | 12 |
| 97:23 | 98:12 | 13 | 115:21 | 116:21 | 24 |
| 98:9 | 98:21 | 12 | 116:0 | 116:21 | 21 |
| 98:12 | 98:23 | 11 | 116:21 | 117:9 | 12 |
| 98:21 | 99:9 | 12 | 116:23 | 117:9 | 10 |
| 98:23 | 99:9 | 10 | 122:21 | 123:9 | 12 |
| 104:10 | 105:10 | 24 | 122:23 | 123:13 | 14 |
| 109:13 | 110:12 | 23 | 130:0 | 130:23 | 23 |
| 110:12 | 111:0 | 12 | 130:23 | 131:9 | 10 |
| 111:0 | 111:20 | 20 | 133:12 | 134:12 | 24 |
| 111:23 | 112:23 | 24 | 134:12 | 134:20 | 8 |

## Results

Drifter data from the third deployment were compared with the AVHRR velocity estimates from April 25 and 26 (Julian days 115 - 116). The images selected are listed in Table 8. Buoy positions were determined from fixes separated by 24 hours. As with the 1993 DCC data, drifter measurements from 12 hours before the initial image to 12 hours after the second image were combined for the comparisons. A plot of the AVHRR-derived versus the drifter velocities is shown in Figure 17. When compared to the drifter velocities, the satellite-derived flow estimates had an overall RMS error of about 18 cm/s and a trigonometric mean error in direction of about 16°. Comparing the interpolated AVHRR velocity estimates with the original drifter vectors gave

16°. Comparing the interpolated AVHRR velocity estimates with the original drifter vectors gave a magnitude ratio (AVHRR/drifter) of 0.30. RMS velocity differences for each image pair/drifter comparison ranged between approximately 17 and 20 cm/s. Directional differences were between approximately 14° and 20° (see Table 9).

**Table 8.** AVHRR image pairs used in the 1994 DCC Experiment velocity estimates.

| Day: Hour | Day/ Night | Satellite | Day: Hour | Day/ Night | Satellite | Time Sep. (Hours) |
|---|---|---|---|---|---|---|
| 115:00 | Night | NOAA 12 | 115:12 | Day | NOAA 12 | 12 |
| 115:09 | Night | NOAA 11 | 115:21 | Day | NOAA 11 | 11 |
| 115:12 | Day | NOAA 12 | 116:00 | Night | NOAA 12 | 11 |
| 116:21 | Day | NOAA 11 | 117:09 | Night | NOAA 11 | 12 |

**Table 9.** Comparison of drifter and AVHRR-derived surface currents for the 1994 DCC Experiment.

| Day:Hour | Ratio AVHRR/ Drifter | RMS Vel. Diff. (cm/s) | Directional Diff. | No. Drifters |
|---|---|---|---|---|
| 115:00 | 0.18 | 17.4 | 13.6° | 12 |
| 115:09 | 0.34 | 18.3 | 18.8° | 37 |
| 115:12 | 0.26 | 19.7 | 14.9° | 48 |
| 116:21 | 0.32 | 17.3 | 15.8° | 61 |

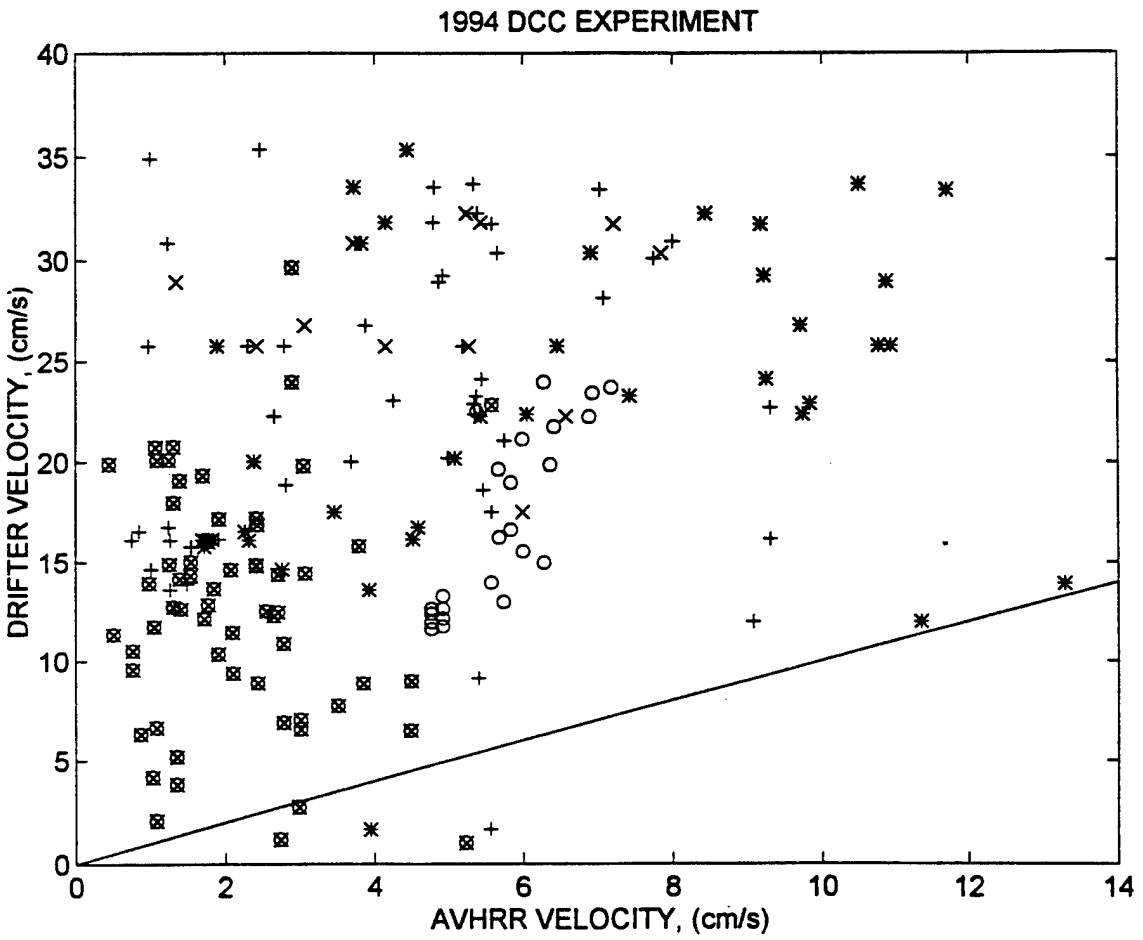


**Figure 17.** Drifter versus AVHRR-derived sea surface velocities for 1994 DCC Experiment: (x) 25 April, 0 Z; (⊗) 25 April, 9 Z; (*)25 April, 12 Z; (O) 26 April, 21 Z.

# 6.0 DISCUSSION

The Cape Race Experiment resulted in a disappointingly small amount of data. This result was not unexpected since the region has particularly adverse weather. On the other hand, the two DCC Experiments provided useful insights into the operational potential of AVHRR for USCG Search and Rescue planning.

Cloud cover is the greatest limitation for using AVHRR images to estimate sea surface currents. Almost all the Cape Race images, 60% of the 1993 DCC and 40% of the 1994 DCC images had clouds covering the entire image. Many of the images identified as completely cloud covered were actually unusable because clouds covered all possible ground control points and the image was not navigable. In the future, navigation algorithms may be improved so that images lacking identifiable ground control points are usable (Rosborough et al., 1994). For an additional 25 to 30% of the time, clouds covered part of the DCC region, reducing the possibility of estimating the surface velocity. Figures 11 and 16 suggest that periods of adverse weather usually lasted 3 to 5 days along the Delaware Coast, but can extend for up to 9 days. Because March to June is usually the best time of year to obtain cloud-free imagery (Clark, 1992), these results may represent the best-case scenario. Although the impact of cloud cover will vary with geographical location and season, it can be expected to severely limit the usefulness of AVHRR for search planning.

Several possibilities exist for overcoming this limitation. One possibility is synthetic aperture radar imagery. Synthetic aperture radar provides all-weather coverage of the sea surface. The Canadian government and NRL are developing algorithms to identify the location and type of surface features on synthetic aperture radar images. Investigations are currently underway to determine if synthetic aperture radar backscatter features are the same as AVHRR thermal features. A second possibility to reduce the effects of cloud cover is to use images separated by more or less than the optimum time separation of 12 hours. Errors in navigation become more significant for image pairs with short time separations, while features may have dispersed if images pairs have long separations. However, it has been seen that the inverse heat equation solution does produce similar velocity fields for time separations other than 12 hours. Linear averaging between cloud-free images is a technique employed by Ocean Imaging of Solana Beach, California. Ocean Imaging provides SST images to commercial fishermen and for oceanographic research cruises. Although this interpolation method is scientifically questionable, Ocean Imaging claims to have obtained reasonable results. NOAA performs a similar procedure for cloud covered regions for its Gulf Stream analysis maps. Its technique is performed manually, and is highly subjective. Although linear averaging is unsuitable for velocity estimation, it can provide a reasonable representation of the sea surface for location of thermal features, a useful capability for search planners. Another possibility is to use GOES, a geo-stationary satellite that provides images at 4 km resolution. Because GOES provides hourly images, scattered clouds may move

across the area of interest, providing views of the sea surface that are masked in the AVHRR imagery. The GOES images may be combined with the AVHRR images to provide a more complete image of the sea surface.

The two DCC Experiments showed that the inverse solution systematically underestimated the surface velocity measured by the drifters. The 1 m drogued drifters used in the 1993 experiment were greatly influenced by the wind so it could be assumed that the drifter velocity would exceed the surface current. However, the drifter design was changed for the 1994 experiment, reudcing the windage, yet the statistical comparison of drifter versus AVHRR-derived velocities was similar for the 1993 and 1994 DCC Experiments. Systematic underestimation of the velocity as measured by drifters has been reported for all AVHRR-derived velocities (for example, Svejkovsky, 1988; Tokmakian et al., 1990; Kelly and Strub, 1992). Kelly and Strub believe this underestimation is inherent in the AVHRR data. They observed drifters moving across thermal boundaries and measuring strong velocities in regions lacking in thermal features. This indicates that knowledge of the heat budget may be insufficient to resolve the horizontal advection in this region. In shallow water and coastal regions, where the DCC Experiments occurred, minimization of the divergence may not be a valid assumption, an assumption inherent in the heat inversion method. The results from the DCC Experiments compared favorably with previous investigations of the inverse and feature tracking methods (Svejkovsky, 1988; Tokmakian et al., 1990; Kelly and Strub, 1992) so they represent the degree of accuracy that can be anticipated for operational use of the inversion method.

An additional source of error is the registration error of ±1 pixel in the spatial registration of AVHRR data. For image pairs separated by 12 hours, this registration error results in an expected current error of ±2.5 cm/s. This error increases for smaller time step size. Other errors occur in regions of local convergence or divergence, where the two-dimensional form of the continuity equation may break down (Wahl and Simpson, 1991). These various sources of error must be considered when attempting to estimate sea surface velocities. The agreement of the current direction was much better than that for the current speeds. Unfortunately, the buoy positions did not correspond to the meanders identified by the AVHRR imagery for in situ comparisons.

The inverse technique for determining the sea surface velocity field has several more physical and mathematical assumptions than feature tracking or pattern matching methods. The inverse technique assumes that the surface temperature gradients extend deep into the water column. While this may be a reasonable assumption during periods of weak vertical shear, during periods of stronger winds when the wind-forced component of surface flow is more significant, the surface flow patterns may be decoupled from the deeper geostrophic flow (Svejkovsky, 1988).

The inverse technique also assumes a simple relationship between temperature and density, so the effect of salinity is therefore assumed to be negligible. This may not be valid near regions of river outflow, strong coastal upwelling, or in highly double-diffusive oceanic regimes (Wahl and Simpson, 1991).

The objective of this investigation was to determine whether AVHRR imagery could improve search planning capabilities. The unquestionable conclusion is that satellite remote sensing can provide a nearly instantaneous picture of the sea surface. As case-dependent data greatly improve the likelihood of target detection, AVHRR-derived sea surface data are a vast improvement over the data currently available to planners. If the area is cloud-free, AVHRR-derived data can provide the positions of current fields, thermal fronts, ocean eddies, and other offshore visibility. By providing cloud cover conditions, AVHRR enables planners to deploy drifters in regions where AVHRR cannot penetrate. Based on the results of this and previous investigations, sequential AVHRR images can provide reasonable surface flow velocities and directions. At present, this is the only method that can produce near-real time, synoptic flow field information over large regions of the ocean surface.

Kelly and Strub (1992) concluded that AVHRR-derived flow fields were useful in characterizing the patterns of circulation and with additional data the AVHRR-derived flow fields could be constrained to produce better overall estimates of the velocity field. Therefore, the inverse technique was developed for ease of incorporating other sources of data. Potential additional data sources include satellite altimetry (see Kelly and Strub, 1992), drifter positions, satellite and airborne synthetic aperture radar and GOES imagery, color scanners (available onboard SeaWiFS - Sea-viewing Wide Field-of-view Sensor) and numerical results. Complementary to this, ISARC is developing a technique to use objective analysis to combine multisource current and wind data to provide high resolution near-real time current and wind data.

# 7.0 OTHER COAST GUARD APPLICATIONS

The objective of this project is to determine the potential of AVHRR imagery for oceanic search planning. However, clearly satellite technology is applicable to other Coast Guard missions. AVHRR-derived SST maps provide data on mesoscale eddies, such as those shed by meanders of the Gulf Stream and other boundary currents, and small-scale phenomena, such as frontal regions and coastal upwelling, information that is valuable in fulfilling Fisheries Enforcement and Marine Environmental Protection (MEP) missions.

## 7.1 FISHERIES ENFORCEMENT

Thermal gradients and flow often control the aggregation of fish (Simpson, 1992a); therefore, fishery operations are most likely to occur at thermal fronts. Additionally, the onset or disappearance of an upwelling event, can indicate a significant change in the fishing potential of a region (Robinson, 1985). Therefore, it is not surprising that commercial and sports fishermen have been using AVHRR-derived maps of ocean thermal fronts since 1975 to locate fish stocks (Cornillon, 1986). Although AVHRR observations only detect the SST signature, it has been found that AVHRR data are sufficiently representative of interior ocean processes to be of use to fishermen and, in consequence, Fisheries Enforcement. Since fishermen have access to AVHRR-derived SST data and base their fishing locations upon this information, clearly the Coast Guard should be utilizing this information to maximize Fisheries Enforcement efforts.

At present, fishermen are only using AVHRR data to locate oceanic fronts. However, near-surface velocity estimation would also be of use for operational fisheries oceanography. The size and life cycle of fish stocks are strongly affected by the structure and variability of ocean currents (Simpson, 1992a). Once it is profitable for private companies to estimate sea surface velocities and distribute the data to fishermen, operational fisheries will utilize this information and the Coast Guard should be prepared to do so as well.

The greatest limitation associated with the use of AVHRR for Fisheries Enforcement is also the greatest limitation for commercial fisheries: the absence of satellite data because of cloud cover. For enforcement of mid or deep water fisheries, AVHRR data may need to be augmented by historical or in situ data. These data can include subsurface temperature, salinity, catch statistics and bathymetric data (Simpson, 1992a).

## 7.2 MARINE ENVIRONMENTAL PROTECTION

Another Coast Guard mission for which AVHRR may be applicable is Marine Environmental Protection. By altering the sea surface skin temperature and the emissivity of the sea surface skin, oil films can affect the brightness temperature measured by AVHRR. However, it is difficult to predict the effect of sea surface oil slicks on AVHRR-derived SST fields. Depending on the thickness of the slick and the ambient atmospheric and surface wave conditions, the observed radiation temperature may be increased or decreased by the presence of an oil slick. Another shortcoming of AVHRR for monitoring oil spill pollution is that the maximum spatial and temperature resolution of AVHRR is the minimum sensitivity necessary to identify and monitor surface oil slicks (Robinson, 1985). It may prove feasible to monitor oil spills using satellite remote sensing. At present, however, airborne radiometry appears to be a more appropriate monitoring technique.

# 8.0 FUTURE WORK

## 8.1 DATA INTEGRATION

An important element of the ISARC project is the use of CASP models, regional models, drifting buoys, and satellite imagery to provide an integrated approach to search area definition. Efforts are underway to modify the drift modules within the CASP program to accommodate SLDMB data and satellite-derived surface current fields. Techniques are being developed and tested to combine sea surface current data from multiple sources into an optimally interpolated current field. The goal is to produce a total integrated picture of sea surface currents using FNMOC data for the large scale, AVHRR-derived currents for the mesoscale, and SLDMB drift data for the small-scale.

## 8.2 OTHER PASSIVE AND ACTIVE SATELLITE SENSORS

IR scanning radiometers will always be limited by their inability to penetrate clouds. The DCC Experiments showed that even during March to June, the optimal period for obtaining cloud-free images, 40 to 60% of the images acquired were completely obscured by cloud cover. Since Search and Rescue operations frequently occur during periods of poor visibility, this drawback severely restricts the use of AVHRR imagery as an operational tool for Search and Rescue applications. Additionally, it is unlikely that future technical development in either color or IR scanning radiometers will increase their oceanographic applications. Therefore, satellite oceanographers have been moving from visible and IR wavelengths to microwave lengths which can penetrate the cloud and give all-weather views of the ocean (Robinson, 1985). In general, passive radiometers observe the properties of the water (such as temperature) while active microwave sensors measure the properties of the surface (such as roughness and wave height). Microwave sensors, such as those aboard ERS-1, ERS-2, TOPEX/POSEIDON and RADARSAT, have proved their potential for all-weather oceanographic measurements. Several satellites carrying all-weather sensors have been launched or are expected to be launched in the 1990's. The European Space Agency's Remote Sensing Satellite (ERS-1), launched July 1991, and the soon-to-be-launched ERS-2, are primarily for oceanographic applications. ERS-1 and ERS-2 carry four sensors, a scatterometer, synthetic aperture radar, the Along Track Scanning Radiometer (ATSR), and a radar altimeter. The Japanese Space Agency is currently orbiting a synthetic aperture radar sensor aboard JERS-1, which like ERS-1 and ERS-2, was developed to satisfy civil and scientific interests. A short-term NASA goal is to develop a sophisticated synthetic aperture radar sensor by the end of the decade that will meet the requirements for the Earth Observing System (EOS) in support of global change research. Two other satellites primarily designed for ocean applications are TOPEX/POSEIDON, launched in 1992, and RADARSAT, a Canadian-led project involving the United States, launched in November 1995.

TOPEX/POSEIDON carries an altimeter, and RADARSAT will carry synthetic aperture radar. These various sensors have the potential to significantly improve the environmental data used by CASP for search planning. In contrast to visible and IR sensors, microwave sensors are still in the developmental phase, so the possible applications for active sensors are as yet unknown (Robinson, 1985).

## Synthetic Aperture Radar

The synthetic aperture radar provides measurements of the directional ocean wave spectra which is probably the most complete single descriptor of the ocean surface. Synthetic aperture radars have the necessary high resolution imaging capability (on order of tens of meters) to detect large-scale oceanographic features, such as current patterns, fronts, eddies, and gyres, principally by their influence on the surface wave field. Ships, ship wakes, and their associated wave trains can also be observed (Robinson, 1985). Synthetic aperture radar is also useful in locating and tracking oil spills (Barock, 1995). However, the mechanisms by which radar backscatter is modulated by ocean mesoscale features are not well understood (Topliss et al., 1994). Synthetic aperture radar reproduces an image of the backscattering strength of the surface, i.e., the surface roughness due to wind events generating short gravity waves and ripples of a few centimeters in length, present in all but the calmest conditions (Robinson, 1985). The relation between ocean surface roughness and radar backscatter has yet to be described mathematically (Topliss et al., 1994). Topliss et al. (1994) describe various meteorologic and oceanographic conditions and their effects on surface roughness. With synthetic aperture radar, different oceanographic conditions can result in similar backscattered images which makes interpretation in terms of thermal features difficult. Researchers (such as La Violette, 1983 and Scoon, 1986) have described features in synthetic aperture radar imagery and attempted to relate them to environmental conditions, but Askari et al. (1993) noted changes in radar backscatter on transects across the Gulf Stream and found that the radar front did not always spatially match the thermal front.

The current generation of synthetic aperture radar imagery allows the best attributes of synthetic aperture radar data to be combined with other imagery sources to produce a synergistic product (Barock, 1995). An example might be the combination of synthetic aperture radar data with co-located AVHRR imagery data. These fusion products are becoming much easier to produce with the availability of user-friendly commercial image software. Much of the utility of synthetic aperture radar depends on the timeliness of the data. Presently, the use of foreign synthetic aperture radar for near-real time applications is not possible. RADARSAT intends to produce fast-turnaround synthetic aperture radar products. However, the minimum turnaround time for a request is expected to be about three days.

## Altimeters

Radar altimeters (carried aboard ERS-1, ERS-2 and TOPEX/POSEIDON) measure the topography of the sea surface. By measuring the return time for a pulse directed toward the satellite sub-point, an altimeter determines the sea surface to altimeter distance. If the height of the satellite is known, then the absolute height of the sea surface can be determined (Robinson, 1985). From sea surface with respect to the geoid, it is possible to estimate ocean currents in which the pressure forces driving the flow are balanced predominantly by the Coriolis force, i.e., geostrophic currents (Robinson, 1985). Although only geostrophically-balanced currents can be determined from sea surface slopes, ocean circulation, mesoscale eddy fields and boundary-current meandering can be observed using satellite altimeters, if they have sufficient height resolution (Robinson, 1985). Satellite radar altimeters also have the ability to provide information related to significant wave heights (from 1 to 20 cm to within 10% accuracy), wind speed and currents (Townsend et al., 1981). The major drawback to radar altimetry is that it provides a single transect rather than a two-dimensional field as is available from AVHRR and synthetic aperture radar. A single track of radar altimetry data provides only the component of current normal to the satellite track and not the total current.

## Scatterometers

Radar scatterometers are oblique-viewing active microwave devices, which measure the intensity of the backscattered radar energy from a broad sea surface area. Since the amplitude of the return signal depends on the surface roughness at length scales comparable to the radiation wavelength, the strength of the return signal can be interpreted empirically as a measure of the sea-surface roughness. Depending on the particular radar wavelength used, the magnitude of the return can be related to either the near surface wind speed (wind-scatterometers), the surface wind stress, or the surface-wave field (wave-scatterometers). By viewing the same piece of sea surface from different directions, a measure of wind or wave direction can be achieved (Robinson, 1985). Synthetic aperture radar operates in essentially the same way, but it is capable of resolution on the order of tens of meters in contrast to the return resolution of a scatterometer of order 50 km (Robinson, 1985). The scatterometers carried aboard ERS-1 and ERS-2 are capable of measuring the wave spectral energy density to within 20% accuracy at 12 discrete wavelengths over a wavelength range between 100 m and 1000 m. The wind scatterometer can measure wind speeds between 4 and 24 m/s to within $\pm$ 2 m/s and direction to within $\pm$ 2 degrees averaged over a 50 x 50 km area.

The microwave sensors described above are all active sensors. The ATSR and the color sensor that will be carried aboard SeaWiFS are both imaging IR sensors, so like AVHRR, are severely limited by cloud cover. However, as data from these instruments are or will soon be available to the oceanographic community, it is worthwhile discussing their potential for oceanic search and rescue.

## Along Track Scanning Radiometer (ATSR)

The ATSR is essentially a multichannel IR sensor, but its conical scan mirror will result in the same piece of ocean being observed twice, once from immediately above and once at approximately 60° incidence. The difference in atmospheric pathlength from the satellite to the surface for the two observations enables measurement of the atmospheric effects. Knowing the atmospheric effects will increase the ability to correct for the atmospheric absorption and emission, and therefore, improve the atmospheric correction algorithms. When averaged over a 50 x 50 km area the absolute accuracy should be within 5° Kelvin (K) and relative accuracy of 0.1° K. The ATSR can produce images with 1 km x 1 km resolution.

## Sea-viewing Wide Field-of-view Sensor (SeaWiFS)

The SeaWiFS aboard Orbit Science Corporation's SeaStar spacecraft (scheduled for launch in summer 1996) is designed to measure eight frequencies in the visible region of the electromagnetic spectrum. It is the follow-on sensor for NASA's Coastal Zone Color Scanner (CZCS); however, SeaWiFS will have a higher spectral resolution and a higher signal-to-noise ratio than CZCS (Simpson, 1992a). SeaWiFS will produce both Local Area Coverage (LAC) and Global Area Coverage (GAC). The LAC data have a resolution of 1.13 km at nadir, will be transmitted continuously while the satellite is in sunlight, and will be receivable at existing HRPT stations (same as for AVHRR). The HRPT stations will require minor hardware modifications and new software for image processing to receive the encrypted SeaWiFS data (Lyon and Willard, 1994). The GAC data are subsampled from the LAC data by selecting every fourth line and every fourth data sample (4 km resolution). The GAC data will be recorded on board the satellite. The GAC data will be downlinked directly to the NASA Wallops Flight Facility and forwarded to the SeaWiFS Science Data and Information System at NASA Goddard Space Flight Center (Simpson, 1992a).

By utilizing both ocean color and sea surface thermal information, the combination of SeaWiFS and AVHRR data will provide a more complete view of ocean surface dynamical processes. In regions such as the Gulf of Mexico where the sea surface loses its thermal signature during the summer months, AVHRR is unable to resolve the surface circulation. However, a color-scanner image of the same region may reveal a strong color signature which may make surface current estimates feasible.

## Combining Sensor Data

In the past the use of a single sensor has provided information never before available on such a large scale. Studies have now progressed to the use of high resolution multichannel sensors with different spatial resolutions where measurements by two or more sensors can be compared and combined, allowing more detailed information to be extracted. Optical and radar data can complement each other in many ways. Comparisons between active microwave sensors and passive radiometers will be particularly useful for oceanographic applications.

The plan is to utilize the advances in satellite remote sensing from synthetic aperture radar operations. The progress achieved thus far using AVHRR imagery has revealed its limitations for all-weather operational use. Unlike AVHRR, synthetic aperture radar can penetrate clouds, haze, smoke, and darkness, providing detailed images of the ocean surface in all weather at any time. Combining data from several sensors, such as AVHRR, satellite altimeters, synthetic aperture radar and scatterometers, will significantly improve the environmental data files used by CASP in terms of all-weather coverage and accuracy. Using a series of images from these various sensors, the SIDSC project plans to develop the techniques needed to combine the data acquired from the radar and IR devices to generate velocity estimates with greater accuracy than is currently feasible from AVHRR imagery alone. Many techniques developed and knowledge acquired in the development of the AVHRR-derived currents will be applied to the radar satellite data. Because the heat inversion technique is based on the SST it will not be directly transferable to radar or color-scanning imagery. Most likely, the satellite altimetry and radar data will be used to improve the accuracy of the velocity fields obtained from the AVHRR imagery.

The first step is to determine if synthetic aperture radar can be used operationally to derive sea surface currents for search planning. The next step is to identify the methods necessary to obtain the oceanographic data (such as wave energy spectrum and winds) from ERS-1, ERS-2 and RADARSAT in near real-time. We will then acquire or develop the techniques necessary to analyze the data and produce near real-time ocean surface currents that can be integrated into the CASP environmental data file using objective analysis. This data will have applications for a Rescue Coordination Center in estimating survival time, suitable rescue craft, and preferred rescue techniques.

# 9.0 OBSERVATIONS AND RECOMMENDATIONS

The three-year development, demonstration, and proof-of-concept program on the potential applications of AVHRR satellite imagery for USCG Search and Rescue missions has been completed. Operational data processing procedures have been examined to increase their speed, accuracy and automation. Three experiments have been performed to determine the feasibility of using AVHRR operationally for search planning and to compare the results of Kelly's (1989) heat inversion technique to drifting buoy measurements. Listed below are some observations and recommendations concerning the design and implementation of an AVHRR-based system for estimating ocean surface currents.

1. Satellite remote sensing can vastly improve the quantity and quality of the environmental data available for search planning. AVHRR-derived oceanographic data have several potential applications that would be useful to the RCCs and other Coast Guard programs such as Fisheries Enforcement and MEP. The value of SST contour maps has already been shown. The technology is available now to generate these maps in near real-time and to distribute them by facsimile to the RCCs or shipboard. Contour maps can aid in locating the position of oceanic fronts and eddies, information that is of immediate interest to the RCCs, Fisheries Enforcement and MEP. AVHRR-derived thermal feature maps can be used to identify the optimal locations for datum marker buoy deployment by providing the positions of fronts, eddies, current features, and cloud cover. AVHRR-derived velocity estimates can provide case-dependent flow data on temporal and spatial scales that are otherwise unobtainable.

2. Data from AVHRR are subject to the following limitations: a) the frequency of useful images is severely limited by cloud cover so that it is not always possible to acquire sufficient data to estimate surface currents, and b) during certain seasons, the thermal structure of the surface water may be lost, making it impossible to acquire surface currents from AVHRR imagery. A related problem occurs when the sea surface and land temperatures are similar so that it is impossible to identify ground control points (GCPs) and navigate the image.

3. Sea surface currents determined from AVHRR imagery lack close-interval sampling in time, and are not as accurate as in situ recording from drifting buoys. However, the satellite data provide a time-instantaneous, spatially continuous portrait of sea surface conditions. Although the positions of SLDMBs can be determined with an accuracy of better than 150 m (Service ARGOS, 1994), the buoy positions results in temporal rather than spatial resolution of the current field. Even with a large array of SLDMBs, the distance between the buoys

may be large compared with the spatial scales of many oceanic features. Surface current maps produced objectively from the buoy data tend to underestimate actual spatial gradients and to present a smooth and misleadingly coherent current field (Garret, 1981).

4. The SIDSC system should be retained at a Marine Science Information Center (MISC) rather than at the RCCs. The SIDSC system will never be completely automated (Kelly, 1992; Strub, 1992). The data processing (in particular, navigation and cloud screening procedures) and the procedures to derive surface currents from satellite imagery are best implemented by human decisions. The SIDSC system will be developed to minimize the need for human intervention but not eliminate it. The experience gained thus far has shown that the efficiency of the system and the accuracy of the results are strongly influenced by operator experience. The ideal operator for the SIDSC system will be trained on the system, experienced with its operation, and will possess a strong oceanographic background.

5. Many preliminary data processing procedures are well suited to automation, thus increasing time efficiency while reducing operator dependence. Some procedures will always require human intervention, not necessarily because the procedure is complex, but because a human is better able to make certain types of decisions than a computer. For instance, navigation of an image will always require human intervention to locate the GCPs. Cloud screening will require human review to verify that clouds have been identified and masked correctly. The heat inversion technique will also require interaction to determine the optimum weighting factor for minimizing divergence and to provide quality control of the velocity vectors. Other procedures, such as the scheduling, preliminary processing and the conversion to SST, are well-suited to automation. Passes can be scheduled, collected, and archived automatically.

6. The turnaround time from the first request for information to the receipt of the product is expected to be a few hours. It is difficult to predict the turnaround time because of the number of variables involved. For instance: how much time has elapsed since the time of notification; climatological conditions (how many relatively cloud-free images are available); how much navigation is required/feasible (depends on cloud cover and satellite position); the size of the image (number of pixels); and the product requested (thermal contour maps require little human intervention and can be delivered much more quickly than a total velocity field). It is possible to estimate the time required to perform many of the procedures necessary to obtain the velocity field. The approximate time to process a single image is 1 to 1 3/4 hours. To estimate the surface currents, at least two images are needed, so the minimum time is approximately doubled.

7. To derive sea surface currents from AVHRR imagery, a system is required to collect the data from the satellite, convert the raw data stream, process the satellite image and analyze the data. This system will consist of a data acquisition module and data and image processing module. The data acquisition module requires a personal computer (PC), satellite antenna

controller, and the satellite antenna and cabling. The data and image processing and analysis module requires a scientific graphics workstation and a printer capable of printing imagery. The data acquisition module is crucial to the operation of the imaging system. If a component of the data acquisition module should fail, satellite data will not be collected, an error that is unrecoverable. A complete backup of the module should be available so that risk of lost data due to computer downtime is minimized.

8. To provide AVHRR-derived data for the entire USCG operating area, it will be necessary to have links to a network of satellite receiving ground stations. These stations do not necessarily need to be owned or operated by the USCG. Many educational, government, or commercial institutions maintain their own satellite receiving stations. Agreements, either financial or data in-kind, would need to be arranged so the MSIC receives the AVHRR data as needed. Processing of the data should remain a responsibility of the MSIC to maintain quality control.

9. The limitations of AVHRR require that the surface currents derived from AVHRR imagery must be supplemented by other measurements during periods of cloud cover. Advances in satellite sensors in the near future (five years) will make all-weather, day and nighttime estimates of sea surface velocities feasible using satellite imagery.

# REFERENCES


Askari, F., G.I. Geernaeft, W.C. Keller and S. Raman (1993) Radar imaging of thermal fronts, International Journal of Remote Sensing, 14, 275-294.

Barnes and Smallwood (1982) TIROS-N series direct readout services users guide, U.S. Dept. of Commerce, NOAA, National Earth Satellite Service.

Barock, R.T. (1995) Littoral warfare from space, Space Tracks, Winter 1995, 2-5.

Breaker, L.C., L.D. Burroughs, T.B. Stanley and W.B. Campbell (1992) Estimating surface currents in the slope water region between 37 and 41° N using satellite feature tracking. Tech. Note, OPC Contribution No. 48, National Meteorological Center, U.S. Dept. of Commerce, NOAA, Ocean Products Center, 47 pp.

Charnock, H. (1985) in Robinson, I.S. Satellite Oceanography: an introduction for oceanographers and remote-sensing scientists, Ellis Horwood, Ltd., Chichester, U.K., 455 pp.

Clark, J. (1992) Personal communication.

Cornillon, P. (1986) Satellite oceanography: a new tool for marine policy makers, Marine Policy, Jan 1986, 57-60.

Davis, R.E. (1985) Drifter observations of coastal surface currents during CODE: The method and descriptive view, J. Geophys. Res., 90(C3): 4741-4755.

Emery, W.J., A.C. Thomas, M.J. Collins, W.R. Crawford, and D.L. Mockas (1986) An objective method for computing advective surface velocities from sequential infrared satellite image, J. Geophy. Res., 91(C11) 12865-12878.

Gallaudet, T.C. and J.J. Simpson (1991) Automated cloud screening of AVHRR imagery using split and merge clustering, Remote Sens. Environ, 38: 77-121.

Gallegos, S.C., J.D. Hawkins, and C.F. Cheng (1993) A new automated method of cloud masking for AVHRR full-resolution data over the ocean, J. Geophys. Res., 98(C5): 8505-8516.

Garret, J. (1981) Oceanographic features revealed by the FGGE drifting buoy array, in Oceanography from Space, J.F.R. Gower, Ed., Proceedings of the COSPAR/SCR/IUCRM Symposium on Oceanography from Space, May 26-30, 1980, in Venice, Italy, Plenum Press, New York, 61-69.

Holland, J.A. and X.-H. Yan (1992) Ocean thermal feature recognition, discrimination, and tracking using infrared satellite imagery, IEEE Trans. on Geoscience and Remote Sensing, 30(5): 1046-1053.

Kelly, K.A. (1989) An inverse model for near-surface velocity from infrared images, J. Phys. Oceanogr., 19, 1845-1864.

Kelly, K.A. (1992) Personal communication.

Kelly, K.A. (1983) Swirls and plumes or application of statistical methods to satellite-derived sea surface temperatures, Code Tech. Rep. No. 18, SIO Ref. No. 83-15, 210 pp.

Kelly, K.A. and P.T. Strub (1992) Comparison of velocity estimates from advanced very high resolution radiometer in the coastal transition zone, J. of Geophy. Res., 97(C6): 9653-9668.

Kidwell, K.B. (1991) NOAA Polar Orbiter Data Users Guide (TIROS-N, NOAA-6, NOAA-7, NOAA-8, NOAA-9, NOAA-10, NOAA-11, and NOAA-12), NOAA NESDIS, Nat. Climatic Data Center.

Kubota, M. (1992) A new cloud detection algorithm, Submitted to J. of Atmospheric and Oceanic Tech.

Lauritson, L., G.G. Nelson, and R.W. Porto (1979 and updates) Data extraction and calibration of TIROS-N/NOAA A-G radiometers, NOAA Tech. Memo. NESS 107, U.S. Dept. of Commerce, Washington, D.C., 58 pp.

La Violette, P.E. (1983) The Grand Banks Experiment: a satellite/aircraft/ship experiment to explore the ability of specialized radars to define ocean fronts, Naval Ocean Research Development Activity Report 49.

Lyon, K.G. and M.R. Willard (1994) SeaStar satellite monitoring of marine and coastal zones for the 1990s, Presented at the Second Thematic Conf. on Remote Sensing for Marine and Coastal Environments, New Orleans, LA, 31 Jan. - 2 Feb.

McClain, E.P., W.G. Pichel, and C.C. Walton (1985) Comparative performance of AVHRR-based multichannel sea surface temperature, J. Geophys. Res. 90: 11587-11601.

Münchow, A.K. and R.W. Garvine (1993) Dynamical properties of a buoyancy driven coastal current, J. Geophys. Res., 98(C11): 20063-20077

O'Donnell, J., A.A. Allen, and D.L. Murphy (1995) An assessment of the errors in Lagrangian velocity estimates obtained by FGGE & WOCE drifters, submitted to J. Atmospheric and Oceanic Technology.

Robinson, I.S. (1985) Satellite Oceanography: an introduction for oceanographers and remote-sensing scientists, Ellis Horwood, Ltd., Chichester, U.K., 455 pp.

Rosborough, G.W., D.G. Baldwin, and W.J. Emery (1994) Precise AVHRR image navigation, IEEE Trans on Geoscience and Remote Sensing, Vol. 32, No. 3, 644-657.

Scoon, A. (1986) An investigation of an ocean front using Synthetic Aperture Radar, MSc Thesis, University College, London.

Service ARGOS (1994) News Flash.

Simpson, J.J. (1992a) Remote sensing and geographical information systems: Their past, present and future use in global marine fisheries. Fish. Oceanogr. 1:3, 238-280.

Simpson, J.J. (1992b) Personal communication.

Simpson, J.J. and C. Humphrey (1990) An automated cloud screening algorithm for daytime advanced very high resolution radiometer imagery, J. Geophys. Res., 95(C8): 13459-1348.

Strub, P.T. (1992) Personal communication.

Sumner, T. (1993) Satellite navigation program for U.S. Coast Guard Search and Rescue Applications, Independent Study Rep., USCGA.

Svejkovsky, J. (1988) Sea surface flow estimation from advanced very high resolution radiometer and coastal zone color scanner satellite imagery: a verification study, J. of Geophys. Res., 93(C6): 6735-6743.

Tokmakian, R.T., P.T. Strub, and J. McClean-Padman (1990) Evaluation of the maximum cross-correlation method of estimating sea surface velocities from sequential satellite images, J. Atmos. Oceanic Technol. 7, 852-865.

Topliss, B.J., T.H. Guymer, and A. Viola (1994) Radar and infrared measurements of a cold eddy in the Tyrrhenian Sea, Int. J. Remote Sensing, Vol. 15, No. 6, 1173-1188.

Townsend, W.F., J.T. McGoogan, and E.J. Walsh (1981) Satellite radar altimeters - present and future oceanographic capabilities, in Gower, J.F.R., ed., Oceanography from Space, New York, Plenum Press, 625-636.

Wahl, D.D. and J.J. Simpson (1991) Satellite derived estimates of the normal and tangential components of near-surface flow, Int. J. Remote Sensing, Vol. 12, No. 12, 2429-2571.

Yu, Y. and I.J. Barton (1994) A non-regression-coefficient method of sea surface temperature retrieval from space, Int. J. Remote Sensing, Vol. 15, No. 6, 1189-1206.